DESIGN OF A ROBOTIC BIO-SAMPLER AND LOCALIZATION IMPROVEMENT FOR UNDERWATER AUTONOMOUS GLIDERS

BY PRATUL KUMAR SINGH

A thesis submitted to the

Graduate School—New Brunswick

Rutgers, The State University of New Jersey

in partial fulfillment of the requirements

for the degree of

Master of Science

Graduate Program in Electrical and Computer Engineering

Written under the direction of

Dr. Jingang Yi

and approved by

_____

_____

_____

New Brunswick, New Jersey

May, 2014

ABSTRACT OF THE THESIS

Design of a Robotic Bio-Sampler and Localization Improvement for Underwater Autonomous Gliders

by Pratul Kumar Singh

Thesis Director: Dr. Jingang Yi

This thesis comprises two parts, the first part presents the development of a robotic platform to function as a biological sampler compatible with the Slocum Underwater Autonomous Glider (UAG). The second part presents a localization algorithm to improve positioning estimation of the glider underwater.

The ocean is very critical to life on earth yet 95% of it still remains unexplored. Hence, scientists all over the world have been deeply interested in understanding all the features of the ocean. One such feature which still remains unclear is how a diverse bacterial community transitions between seasons in a coastal ecosystem and how this transition affects the global biogeochemical cycles. This is because of our inability to collect water sample at the right time and space in these ecosystems to resolve the processes influencing the microbiota. One of the reasons for this inability is the lack of a component capable of collecting and returning intact biomass to the laboratory for molecular ecology studies. To meet this requirement, the first part of this thesis aims at development of a robotic platform called the bio-sampler to address fundamental questions in marine ecology and to elucidate the mechanisms supporting the diversity of microorganisms in the ocean. Our aim is to have the bio-sampler installed in the science bay of the glider. Such a mobile platform is capable of in-situ sampling and preservation on a range of spatial scales. Using the bio-sampler

we demonstrated autonomous filtration of samples and running our preservation process on them. We also conducted contamination and sample preservation tests to validate the functioning of this robotic platform. The results confirmed that the bio-sampler was able to perform sample preservation without carrying any water sample from previous sample to the next one. The results also confirmed that the bio-sampler did not cause any cross-contamination between samples.

In the second part of this thesis, we try to improve the localization of the Slocum glider. Underwater autonomous gliders such as the Slocum glider provide an effective platform for marine and coastal scientists for conducting exploration missions which may last several weeks or even months. However, localization of these gliders underwater is a challenging task based only on the sensors on-board these gliders. Also these gliders move slowly, with an average horizontal velocity of around 0.2 - 0.3 m/s and hence are vulnerable to ocean currents. When these gliders resurface, they receive GPS signals to identify their position. Since they mostly run underwater this makes it difficult to obtain accurate positioning of the glider. The new localization scheme is based upon the dynamic model of the glider fused with on-board sensor measurements like depths and yaw angles. The experimental results have shown that the new localization scheme improves the position estimation of the glider without using any new sensors apart from the ones which are already on the glider.

List of Figures

List of Tables

Acknowledgements

I thank my advisor Dr. Jingang Yi, whose guidance enabled me to pursue this study. I would also like to thank Dr. L. Kerkhof, and Dr. S. Tuorto, Mr. D. Aragon ,and other RUCOOL members from the Institute of Marine and Coastal Science at Rutgers University for their invaluable discussions and suggestions. I also want to extend my thanks to Dr. U. Kremer and Mr. C. Woithe of the Department of Computer Science for their discussions on the problem of glider localization. Further, I would like to express my gratitude to my lab mates Pengchang Wang, Adam Caretta, Mitja Trkov, Moiz Ezzy, Ian Abraham, Gabriel Azaceta and every other lab mate for their inputs on the project. I would also like to thank John Petrowski for introducing me to the 3D printing technology and speeding up my prototype development. Also I would thank Dr. Zoran Gajic and Dr. Quingze Zou for supervising my thesis defense. Finally, I would like to thank the Departments of Electrical and Computer Engineering and Mechanical and Aerospace Engineering at Rutgers University, for providing the necessary research infrastructure.

Table of Contents

Chapter 1

Introduction

The coastal and marine science community is interested in understanding the dynamics of microbial bloom especially on the continental shelves. The reason for their interest in these coastal ecosystems is due to the fact that they have an impact on global biogeochemical cycles, despite their relatively small size. Research done by the marine scientists at Institute of Marine and Coastal Science at Rutgers University have shown that in between seasons, there is a profound shift, with the replacement accounting to approximately 50 % of the bacterial community by a new group of micro-organisms. Also important to note is that such alterations occurred within a short time span which were lesser than 3 weeks. The knowledge about such diverse bacterial community transitions observed in short time periods is difficult to obtain. The reason for this lies in our inability to collect and preserve water samples in time (e.g., monthly, seasonal, annual) and spaces (e.g., boundary current, eddy, gyre, coastal areas) scales which would help us unravel the processes affecting the microbiota.

In order to overcome this inability, we have proposed a design for a robotic biological sampler, called the bio-sampler, which can be installed on the Slocum glider. The Slocum glider is an Underwater Autonomous Glider (UAG) for ocean research and monitoring capable of moving to specific locations and depths. It has been employed by the marine scientists at Rutgers University to map physical, chemical and bio-optic properties in oceans around the globe. These gliders are battery powered and have buoyancy mechanisms that help it to dive and ascend. The glider uses hydraulic buoyancy change to alter the density of the vehicle with respect to the surrounding water thereby causing it to sink or float. Therefore the gliders flight path has a saw-toothed profile underwater. This can be seen in Fig. 1.1. Slocum gliders use these mechanisms to change buoyancy only around the inflection points in their flight path. Hence these gliders consume very less energy compared

to other Underwater Autonomous Vehicles (UAV) which are powered by propellers and are constantly steered by running the propellers. The on-board battery packs can thus last several weeks or even months without an interruption while on a mission. With the on-board science bay sensor suite such as pressure sensor, temperature, salinity and density (CTD) sensor, etc., the marine and coastal scientists are able to sample underwater in both spatial and temporal scales [2]. The flexibility of this glider to change the science bay sensors make it versatile for optimizing the glider as per mission requirements.

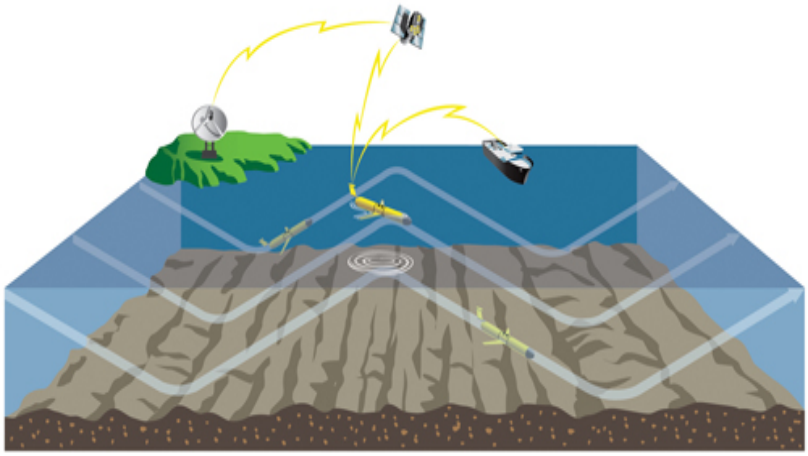

Figure 1.1: Flight path and communications of a Slocum Glider [1]

We propose to design a robotic bio-sampler which can be mounted in the science bay of the glider and sent on a mission. This would provide us a platform capable of sampling, preserving and returning intact biomass to the laboratory for molecular ecology studies and thereby help us understand the microbial bloom dynamics.

Working in this direction, the design process was primarily focused on a mechanism that would use multiple filters for sampling in an autonomous way. During initial meetings, we discussed about various mechanisms like the bottle-filling stations, a platform full of filters, and the use of a robotic arm to transfer water samples, etc. Also while deciding the design of the bio-sampler we had always considered the space and power constraints on the glider. The dimensions of the science bay on Slocum glider is approximately 11 inches long and 8 inches in diameter. However, in order to validate our design we eliminated these two constraints and started building the system. Hence we chose the power supply to the

bio-sampler to be given via a general AC supply using an AD-DC adapter. Eliminating the size constraint we decided to go with a table-top version of the bio-sampler first. As the main working principle, we chose a rotation based mechanism to shift from one filter to another, and a clamping mechanism for sealing the filter and drying the water off the filter. Our idea was to design a system that would perform the main functions of sampling and preservation of biomass first. After this is achieved we would modify the design to adapt it to make it compatible with the glider.

The set up of having a bio-sampler mounted in the science bay of the glider is advantageous from the point of view of capturing samples during these biological transitions. Rutgers University is one of the largest operators of these gliders in the world. Having a robotic bio-sampler on this glider integrates their experience of maneuvering the glider to a desired location with the autonomous sampling and preservation of biomass at that particular location. This combines the advantage of the glider in occupying controlled spatial and temporal grids with that of the bio-sampler to conduct sampling in these regions of biological interest. The natural slow speed of the glider and a fast sampling of water would give a high resolution spatially and temporally in obtaining biomass for laboratory analysis.

The Slocum gliders lack inexpensive and effective localization sensors. The glider mainly uses dead reckoning algorithm for localization while on a mission underwater. This technique suffers from being simple and not capable of capturing actual uncertainties such as ocean currents. The glider's horizontal velocity being around 0.2-0.3 m/s makes it vulnerable to ocean currents which may have velocities in around 0.06 m/s underwater and ever higher surface velocities. When the glider resurfaces during the mission, it localizes itself through the on-board GPS and continues to the next commanded locations. The positioning information is critical for exploration. As pointed out earlier, to take advantage of this combination of a bio-sampler on board the glider, the glider should be able to reach and localize itself to the exact location of interest. This increases the resolution of sampling when underwater. Hence a new inexpensive localization approach is required in order to achieve our goals.

We propose a new localization scheme which is built on the glider's dynamic model and fused with the on-board sensors. The main idea behind our scheme is to precisely capture

the dynamics of the glider navigation and with the known inputs to the glider, the dynamic model should predict its position. To improve this dynamic model-based positioning approach we designed an Extended Kalman Filter (EKF) to integrate the dynamic model with sensor measurements such as depth and pitch angle. This can also be further enhanced by predicting ocean currents and varying the control inputs in order to compensate for it. We also validated our approach using the experimental data of previous glider deployments done by the Rutgers University Coastal and Ocean Observation Lab (RUCOOL).

The main contribution of this thesis is twofold. First, we develop a table-top version of an autonomous robotic bio-sampler which is targeted to be installed in the science bay of the glider. We have demonstrated the autonomous operation of sampling and conducted cross contamination and preservation tests using the bio-sampler. The results of these tests confirm that the bio-sampler was able to preserve the biomass through the process of drying. Also the results have shown that the bio-sampler was not carrying any remains of the previous sample while moving on to perform the next sampling. To the best of our knowledge, this bio-sampler has several advantages over the ones which already exist such as, being able to concentrate and preserve sample, being automatic, portable, low power consuming, etc. Moreover the biggest advantage of this bio-sampler would be once it is a part of the glider installed in the science bay. Secondly, we propose a dynamic-model based localization approach using no extra sensors except the ones on-board the glider. The experiments also confirm a better performance of our approach than compared to the existing approach. This localization scheme can be further enhanced to estimate ocean currents with sensors such as inertial measurements units (IMU).

The remainder of the thesis is organized as follows. Chapter 2 reviews the related work and describes the motivating factors behind this research. The overall stages of development of the bio-sampler are discussed in Chapter 3. Chapter 4 presents the proposed localization scheme including the dynamic model, EKF design and the results verified by actual previous glider mission data. Conclusion and future work are reported in Chapter 5.

Chapter 2

Background and Motivation

This chapter provides a background of the related work and the motivation to explore the need for a robotic bio-sampler. We discuss the existing similar platforms and compare the features of those with our prototype.

UAGs like Slocum provide an effective platform for marine and coastal scientists to conduct prolonged ocean exploration missions that could last several weeks or months [2–4]. The Slocum glider's trail is similar to a saw-tooth wave. It uses battery-powered mechanisms to move and shift the weights to change buoyancy to descend and ascend underwater. Since the glider only uses these mechanisms around the inflection points during navigation, less energy is used compared to that of other underwater autonomous vehicles (UAV) powered by propellers. Taking advantage of the low energy consumption of the buoyancy engine and the other devices, these gliders can go on a mission that may last for several weeks or months without interruption. Therefore, these gliders are well suited for prolonged ocean exploration missions compared to other types of UAVs . When the glider re-surfaces after a dive, it recognizes its actual position by the on-board global positioning system (GPS). While on surface of the ocean it also communicates with the command center for navigation and data transmission. Because of the operation mechanism, Slocum gliders have slower speed (forward speed around 0.2-0.3 m/s). This causes the glider being vulnerable to environmental disturbances such as ocean currents in terms of navigation. This provides an opportunity to improve localization of these gliders. The positioning information is critical for better oceanic exploration and for rescue missions of these gliders in case they are lost. Hence, it is imperative that we improve the localization of these gliders. Having a bio-sampler on board the glider which localizes better than that at present, will significantly improve the sampling capabilities of the marine scientists.

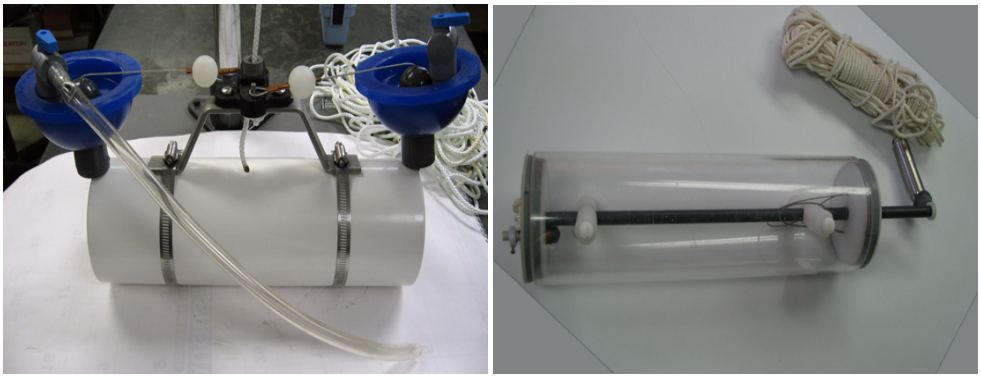

(a) (b)

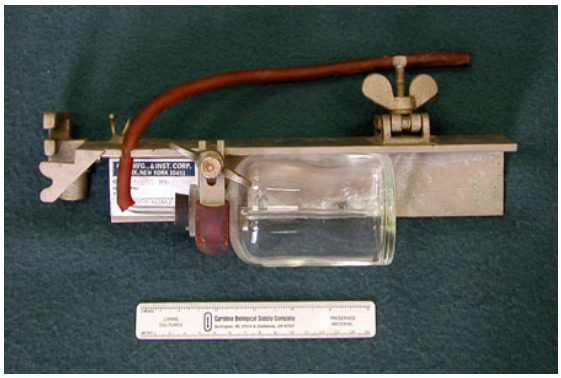

(c)

Figure 2.1: (a) Van Dorn water sampling bottle [5] (b) Kemmerer water sampler [6] (c) JZ Bacteriological Bottle [7]

This chapter provides background and motivation for the two problems that we discuss and these are (i) development of a robotic bio-sampler and (ii) improving localization of Slocum - underwater autonomous glider. For the ease of understanding, this chapter is divided into two sections in which these problems are discussed separately.

2.1 Bio-sampler Design

There are various kinds of bio-samplers that are used by the marine science community. Some are simple which only collect water samples and are brought to the lab for later analysis. Whereas some are complex which carry out biological analysis remotely at the site of sample collection itself. Some oceanographers use simple water sampling bottles which are available on the vessel while on a mission. Examples of such water samplers are like the Van Dorn water sampling bottle, Kemmerer water sampler, JZ Bacteriological

Bottle, etc. shown in Fig. 2.1. These are simple water samplers which only collect water samples at a particular depth. These water samples are then taken to the lab for analysis. Also these samples require a person to handle and carry out the sampling while on-board a vessel or in the field.

An example of a more advanced water sampler is the Gulper which was developed for the Dorado Autonomous Underwater Vehicle (AUV) by Monterey Bay Aquarium Research Institute (MBARI). This is mounted on the AUV as shown in Fig. 2.2. It comprises of an array of 10 syringe-like water samplers. Compared to simple water samplers shown in Fig. 2.1, the Gulper is able to collect water samples underwater at locations where the AUV can be maneuvered to. Each of these samplers can collect two liters of water sample. However this device also only collects water sample but does not perform any filtration or preservation of water samples [8]. After the mission is completed, these water samples are analyzed either on-board the carrying vessel or brought back to the laboratory for analysis.

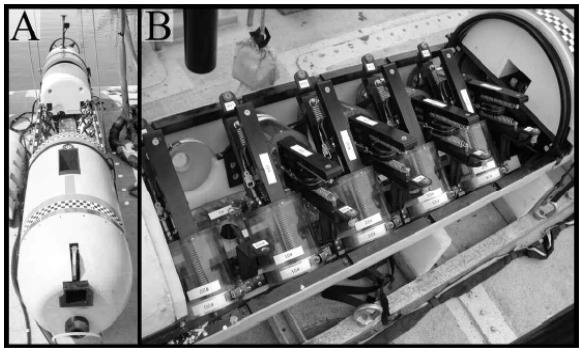

Figure 2.2: MBARI's Gulper sampling system for Dorado AUV [8]

Similarly there are advanced samplers like the Environmental Sample Processor (ESP), also developed by MBARI, which are more complex and provides on-site sample collection and conducts various chemical tests while at sea [9]. It has the capability of collecting a range of water samples varying from milliliters to 2 liters. It has advanced sensor arrays and can perform real-time genetic and chemical analysis of organisms in situ. An electromechanical cable connects the ESP to a radio on the surface float through which it receives commands and transmits data. The whole assembly weighs over 370 kilograms (>800 pounds).

Also similar work has been done by Dr. Steve Tuorto et al. from Institute of Marine

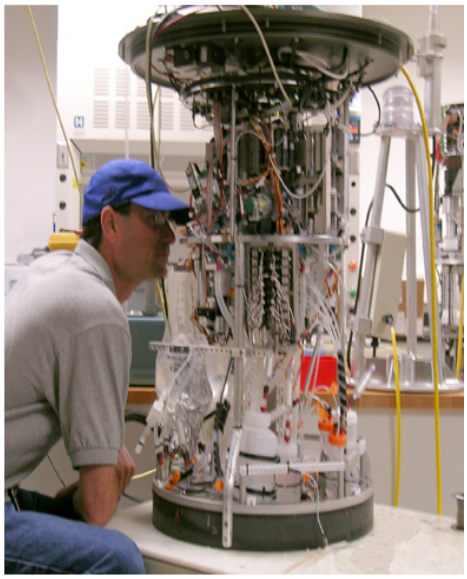

Figure 2.3: MBARI's 2G ESP sampling system [9]

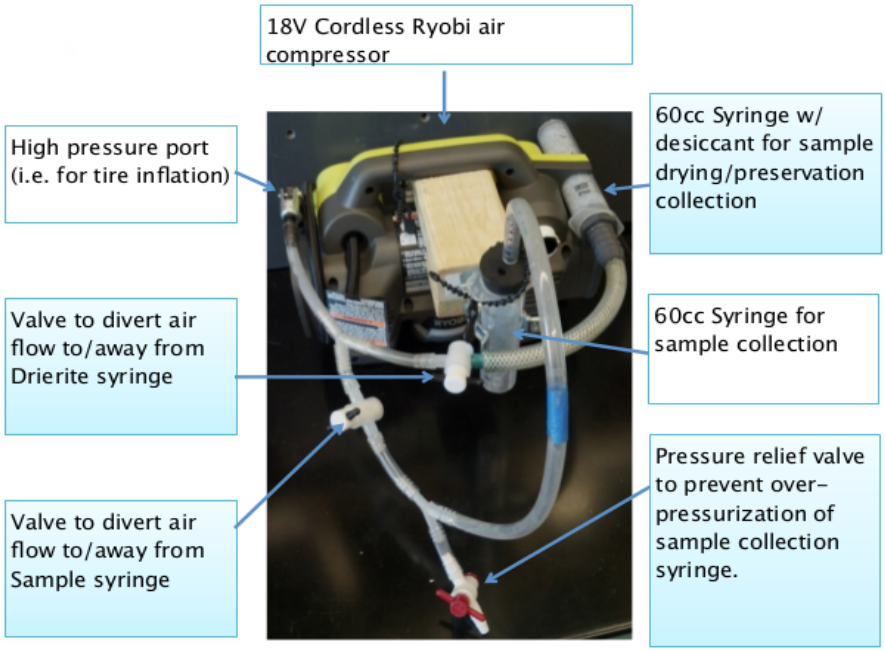

Figure 2.4: BioDry® developed at Institute of Marine and Coastal Science at Rutgers University

and Coastal Science at Rutgers University. Their technique called the BioDry® as shown in Fig. 2.4 is an inexpensive yet effective method of preservation. This apparatus is also portable and has been field tested to show good results. However, it requires manual intervention since this is not an autonomous system.

The developed bio-sampler in this thesis is targeted in between the Gulper and the ESP. Similar to the Gulper, the proposed bio-sampler is installed on the AUV and preserves the bio-mass collected on-site, like the ESP, but for a later analysis in the lab. The bio-sampler would be installed in the science bay of the Slocum glider. This glider would then be sent on a mission and will be programmed to take water samples, filter and preserve them at locations of interest. Hence the gilder-compatible configuration provides the bio-sampler with the advantages in terms of increase in functionality compared to the Gulper but being lesser complex than the ESP.

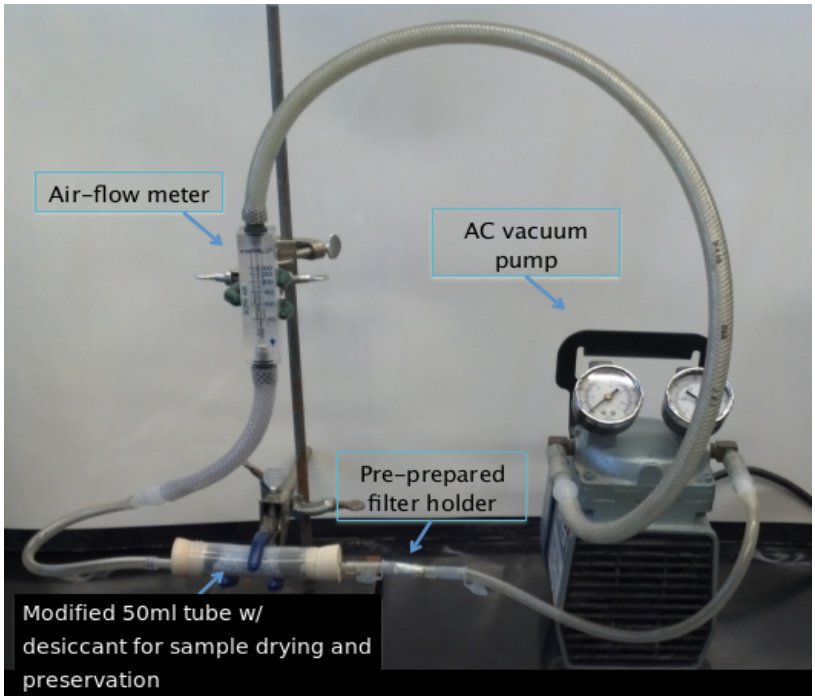

Figure 2.5: Drying and preservation apparatus used by marine scientists: AC powered vacuum pump used to dry a filtered sample.

Currently, sampling is done manually by the marine scientists in the lab using tubes, filters, pumps, etc. Fig. 2.5 shows the drying stage of the sampling procedure used by marine

scientists at Rutgers University. This sampling methodology constantly requires manual intervention and is a slow process vulnerable to a number of human errors. Therefore it is desirable to automate this entire process and improve the process robustness and repeatability. Our goal was to develop the prototype with a simple working principle as a proof of concept of our design. The procedure of the bio-sampler prototype is to autonomously perform pumping the sample water, collecting biomass by filtration, and preserving it by drying the sample for later analysis. Having such a system would help standardize the procedure of sampling and preservation and eliminate any possibilites of errors when sampling and preservation of the water sample is carried out. It is an enabling tool for the marine scientists such that they would focus completely on analyzing the sample rather than spend time in trying to figure out if anything goes wrong at the sampling stage. Therefore the bio-sampler device would tremendously increase the throughput and quality of a lab process in terms of the number of samplings and sample repeatability achieved in a stipulated amount of time.

Table 2.1: Comparison of similar bio-samplers with the Bio-Sampler

	Functions	Gulper	ESP	BioDry®	Bio-Sampler
	Automated	Yes	Yes	No	Yes
	Filtration	No	Yes	Yes	Yes
	Filtrations per hour	NA	no data	4	4
	Portablilty	No	No	Yes	Yes
	Low Power	Yes	Yes	Yes	Yes
	Preservation	NA	Yes	Yes	Yes
	Size (table top)	No	No	Yes	Yes
	Water Collection	Yes	Yes	No	No
	On-Board Analysis	NA	Yes	No	No

2.2 Improving localization of Slocum gliders

Our final goal is to have the bio-sampler on-board the Slocum glider. The localization of these gliders underneath the sea surface remains a challenging task. This is due to the lack of effective positioning sensors in an underwater environment. Also, since the motion of these gliders is in a saw-toothed path with a slow horizontal velocity, these gliders remain susceptible to ocean currents. Using the sensors on-board the glider, the marine and coastal scientists are able to sample the areas underneath the sea surface. Proper localization of the glider is critical from the point of view of conducting sampling at a specified location of interest. Therefore an effective and inexpensive method of localization of the gliders is necessary. This requirement motivates the second part of this thesis which is improving the localization of the Slocum glider.

Motion planning and control of gliders which include the effect of ocean currents are reported in recent years [14], [15]. In [13], a dynamic model for underwater gliders is developed based on Newtonian mechanics. In this work, the author has done experiments to identify and calculate the model parameters for Slocum gliders but no experimental validation of the developed model with glider flight data is reported. In [16], steady turning motion for underwater gliders is obtained using the model developed in [13] but no experiment is reported to validate the analysis. Dead reckoning technique is commonly used for localization. The accuracy of the dead reckoning approach suffers from many simplifications and uncertainties, such as the dead reckoning sensor accuracy and disturbance from unknown ocean currents. Other positioning sensors such as Doppler Velocity Log (DVL) or Acoustic Doppler Current Profiler(ADCP) are expensive and sometimes not reliable due to complex environmental conditions. Most glider systems are not always equipped with DVL or ADCP [3]. In [17], DVL measurements were used to enhance the localization accuracy by dead reckoning. In [18], a model-based navigation system is developed to estimate the ocean currents for underwater vehicles. Our work is inspired by the concept developed in [18]. The navigation system in [18] is designed for propeller-powered underwater vehicles and fused with on-board inertial navigation systems (INS).

We extend the model in [13] and develop a dynamic model for Slocum gliders using

Lagrange's equations. We take the new dynamic model we developed and design a model-aided, EKF- based localization scheme to fuse measurements obtained from several commonly used on-board sensors with known control inputs. More importantly we validate our design using previous glider flight data obtained from the RUCOOL Lab.

In the next chapter we discuss the first part of this thesis which is based on the bio-sampler design.

Chapter 3

Bio-Sampler Design

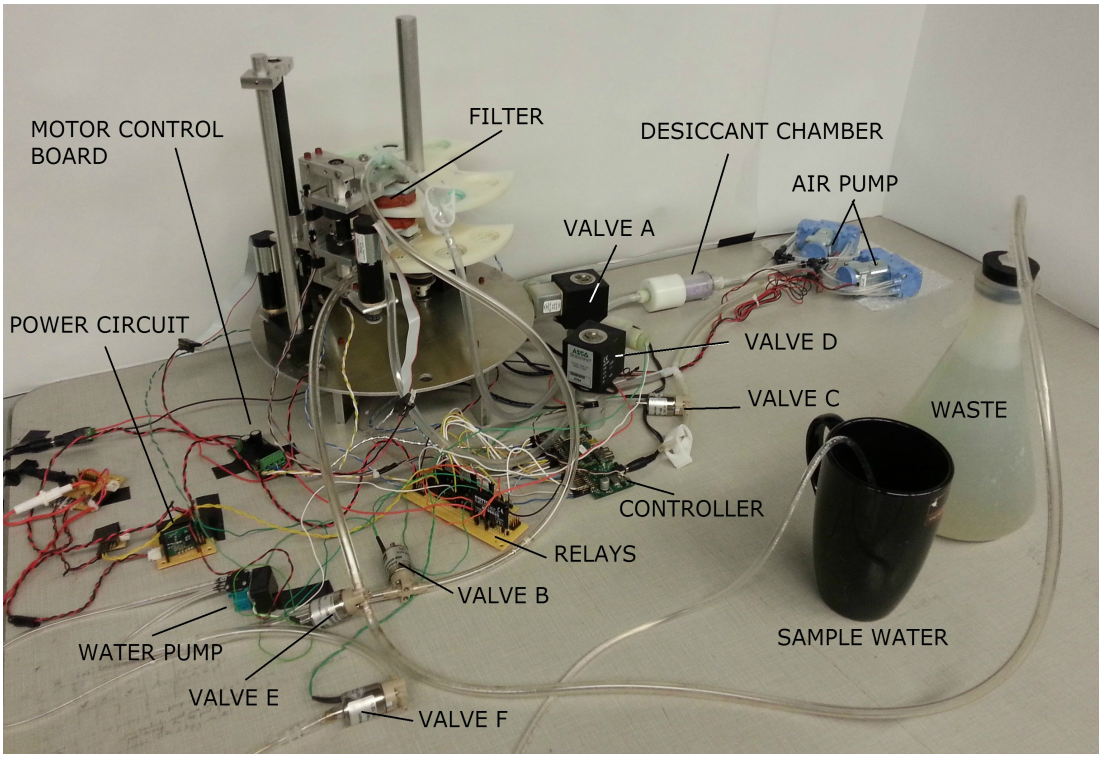

Figure 3.1: Current Bio-Sampler setup

3.1 Origin of the Design

Fig. 3.1 shows the current setup of the bio-sampler. This is the third version of the bio-sampler that we have designed. However, the bio-sampler design went through a series of modifications and rigorous testing before we reached the current working design. This chapter captures the evolution of the design of the bio-sampler from all possible perspectives.

Because of the functional requirements of the bio-sampler, we started with a design that

would fit in the science bay of the Slocum glider and consume low energy. Also in order to increase the throughput in terms of number of samples per deployment, our design should accommodate multiple filters in the bio-sampler. Most importantly, the design must be able to perform two basic functions autonomously. First, it must be able to filter water sample and concentrate the biomass on top of the filter. Secondly, the bio-sampler must be able to preserve the collected biomass. Our method of preservation was based on using effective drying by a combination of air flow and a desiccant, which is a working method used by the marine scientists. Having these requirements as guidelines, we were able to have had an initial design as shown in Fig. 3.2.

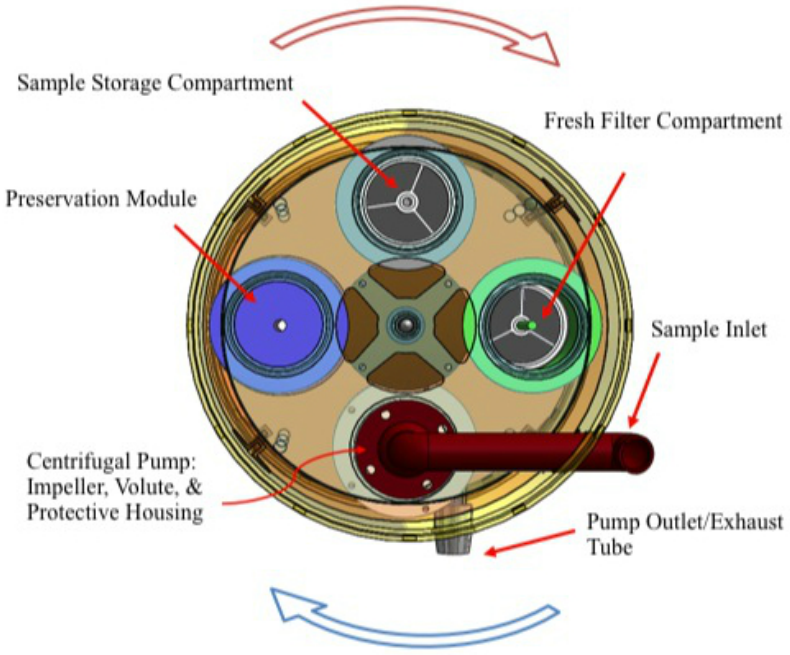

Figure 3.2: Sample Recovery System: Front view [10]

The initial design consisted of compartments similar to the ESP but it had only four of them, each having an individual function. One was to store fresh filters, another one to execute filter preservation, the third one to store the preserved samples and the last one was actually used to sample the water.

The design of functionally dedicated compartments required complicated means of handling the filters while sampling. The complexity of the rotational mechanism led us to

simplify our design. Finally we came up with a design in which multiple filters would be mounted on a filter bracket. Fig. 3.3 shows the design of the central rotating shaft with filter brackets and a clamp mechanism.

3.2 Principle of Operation

The bio-sampler is divided into three subsystems as shown in Fig. 3.3. (i) A set of filter brackets mounted on a central rotating shaft. (ii) A clamp mechanism to seal the filter while filtration and drying is carried out. (iii) A linear actuator to guide the clamp from one filter bracket to the other.

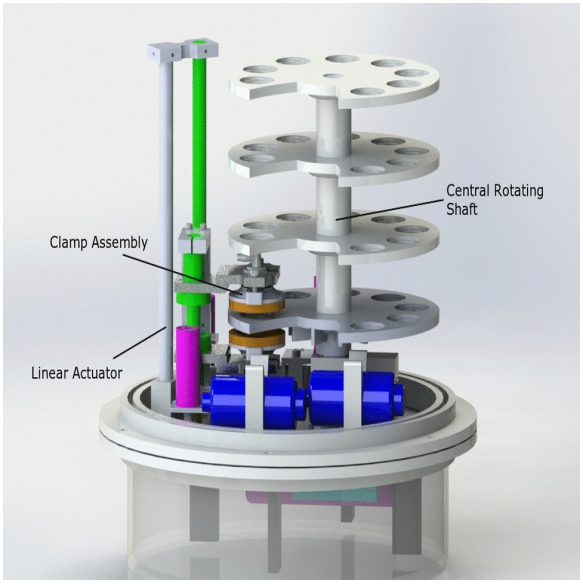

Figure 3.3: SolidWorks™ model showing the 3 DOFs

The clamp is manipulated towards a filter at the desired location. This is achieved by first moving the clamp to the desired filter bracket location. The motion of the clamp to reach one particular filter is achieved by rotating the central shaft to the respective filter location within the chosen filter bracket. After the clamp reaches the desired filter, the clamp closes and seals the filter. Filtration of the water is started using a diaphragm water pump. The pump pushes water from the water source onto the filter via a tube and the outlet water exits from the other side of the filter. The pumping of water through the filter

makes the concentration of the biomass left on the filter possible. Once the filtration is completed, the water from the tubes is purged out by taking in air through the water pump inlet. By doing so, all the water lines are cleared off any traces of previous water sample. Once the water is purged out of the system, the drying stage of the sampling process is initiated. The air flows from the air pump onto the filter and back into the air pump again, thus forming a closed loop of air flow. The air flows around the filter from the air pump via a desiccant chamber which houses a drying agent (Drierite®in our case). Thus the air is desiccated each time it goes through the desiccant and onto the filter for better drying.

3.3 Mechanical Design

3.3.1 Filter used

The filter used for collectiong samples is the same as the one used by the marine scientists for their microbiological analysis. It is a Supor®PES Membrane disc filter as shown in Fig. 3.4. The filter is 25mm in diameter and has a pore size of 0.2μm. and a thickness of 145μm.

Figure 3.4: Supor®filter: Diameter - 25 mm, Pore Size - 0.2μm., Thickness - 145μm.

3.3.2 Linear Actuator Design

The linear actuator can be considered as the first degree of freedom of the bio-sampler. The purpose of the linear actuator is to take the clamp from one filter bracket to another. It mainly consists of a screw rail and a platform that travels when the screw rotates. The clamp assembly is mounted on this platform. A geared DC motor is coupled to the screw of the linear actuator using which the entire clamp assembly fixed to this screw rail can then be positioned with respect to any filter bracket. The initial design of the linear actuator mechanism is shown in Fig. 3.5 (b). This design did work as intended in positioning the clamp assembly with respect to the filter brackets. However it was not very accurate due to the fact that all the parts of this assembly were hand made except the screw. This resulted in imperfections in terms of tolerances that must be maintained when all these parts were assembled together. Hence when the linear actuator was operating the screw would not rotate concentric to the coupling and as a result of which the clamp assembly mounted on this would wobble during travel. This resulted in improper positioning of the clamp and hence it did not provide a perfect seal around the filter. Also another harmful effect of this design was that the clamp would start to bend the filter brackets and the shaft due to the torque created while clamping at a wrong position.

It was a difficult part to machine as it needed very good precision and high level of tolerances. This made us very clear that in the next design we must use a precise linear actuator from a vendor rather than machine one on our own. Precise functioning of this part is necessary because further operations after clamping such as, filtering and drying are directly dependent on the positioning of the clamp with respect to the filter brackets.

In the second version of the bio-sampler the linear actuator was a bought-out item as seen in Fig. 3.6, unlike the one machined in the previous version. This gave us a smoother and a more precise system of aligning the clamp with the filter brackets. Also the torque requirements of the DC motor to run this dropped drastically.

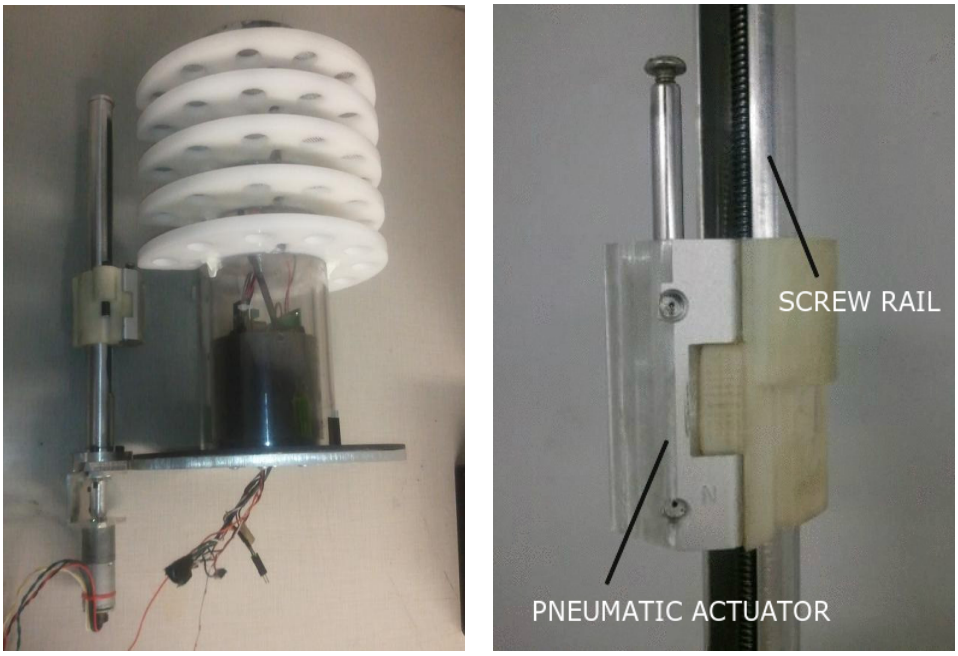

(a) (b)

Figure 3.5: Bio-sampler prototype 1 (a) Central Tube showing the inner motor mount assembly with linear guide on the left and 5 filter brackets (b) Linear Actuator

3.3.3 Rotating Filter Bracket Design

The rotating filter bracket represents the second degree of freedom for the bio-sampler. It has a set of filter brackets or filter brackets which have circular slots for filters to sit on. This rotating shaft helps position the filters with respect to the clamp.

Initial design of the central shaft is shown in Fig. 3.5 (a). The central rotating shaft had 5 filter brackets mounted on it. Each filter bracket in turn had 10 filter rings that supported the filters. Hence the first version of the bio-sampler could handle 50 filters in total. Each of the filter brackets were mounted on a central plastic tube. This entire assembly was then mounted on the shaft of a geared DC motor. The rotating shaft had contact with a very low friction material at the base to assist in a smoother rotation. The central tube also housed the main motor and the motor control boards for both the main motor and the linear actuator motor.

The next version was made to improve upon the limitations from the previous design. This version was more focused upon being sturdy and having the filter brackets removable. An important step before starting the sampling process is to clean the filter brackets before

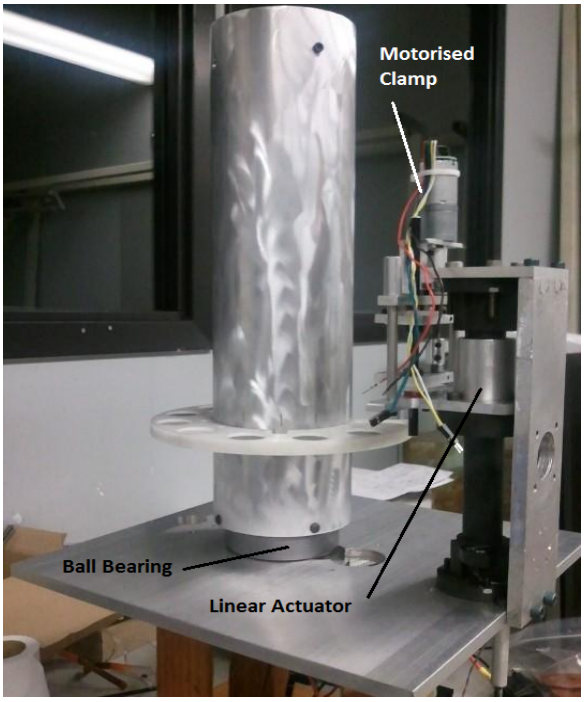

Figure 3.6: Biosampler Prototype 2

we fix the filters into filter slots. If they are not kept clean then the samples would contaminate the next set of samples. Having filter brackets removable made it easy to clean them using chemicals like ethanol. These filter brackets were mounted on the central tube using only three screws. The central tube's plastic body was replaced by an aluminum one as it was more sturdy. Another drawback that the previous design suffered from was the central tube rotating on the low friction base. This did not work very well since the entire weight of the central rotating shaft was on this surface and after a few runs this started to wear-out and the rotations were no longer smooth and regular. This directly resulted in difficulties in positioning the filters with the clamp. Based on these observations, the central tube was now mounted on a bearing which made the rotations smoother compared to the previous design.

The third and the current version of the central rotating shaft was severely cut down in weight, size and complexity. This can be seen in Fig. 3.7. The central shaft is a simple aluminum rod which is designed to fit onto a small bearing. The size of the bearing was considerably reduced as the entire weight of the filter brackets was also reduced a lot. A

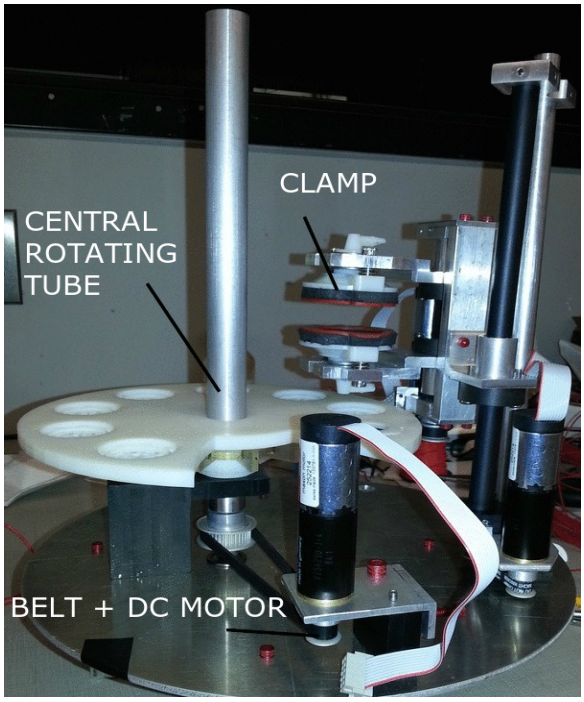

Figure 3.7: Biosampler Prototype 3

geared DC motor is used to rotate this central shaft. However, unlike the previous designs, this version used a toothed belt to couple the shaft with the motor. This version however has only 4 filter brackets and each filter bracket has 8 filter slots for the filters. Also the most important change was taking advantage of the latest technology of 3D printing instead of machining each bracket. The design of the filter bracket became so important and complicated in the end that it is discussed in another section dedicated completely to filter bracket design.

3.3.4 Clamp Design

The clamp constitutes the third degree of freedom for the bio-sampler. It consists of two clamp plates moving in opposite directions during operation. This was one of the most sophisticated parts of the whole system as well as the the most important one. The application of the clamp mechanism is to clamp the filter and seal it during filtration and drying.

Initial design of the clamp was planned to be actuated pneumatically. A pneumatic

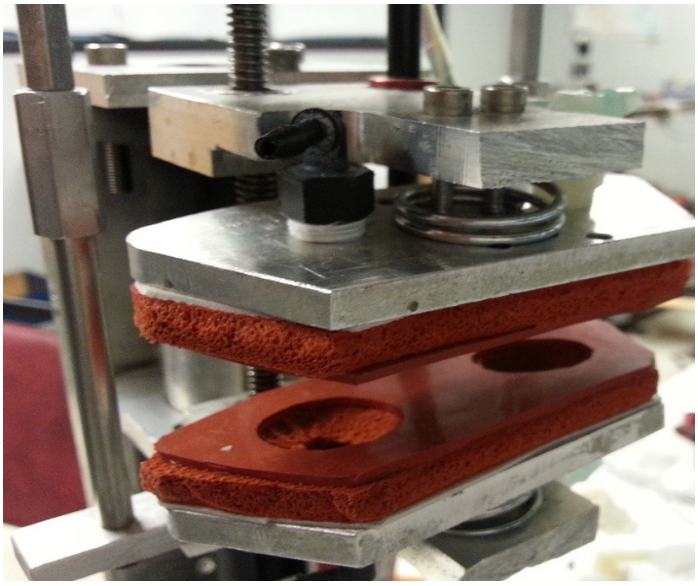

Figure 3.8: Double-headed clamp

actuator is shown in the Fig. 3.5 (b). However this clamp never reached an operational stage since the idea of a pneumatically actuated clamp was too difficult to implement. The later version of the clamp was a two-headed clamp as shown in Fig. 3.8. Each head had an adapter fixed to it so that a tube could be attached to each one of them. One of the head was dedicated for water flow and the other was dedicated for air flow. The clamp assembly was mounted on the linear actuator platform. The clamp can either be opened or closed, when the clamp plates moved away or came closer to each other. The screw was coupled to a geared DC motor shaft using a coupler. When the motor rotated the coupled screw also rotated and the clamp would either open or close based on the direction of rotation of the motor.

Clamp Redesign - Double headed clamp to Single headed Clamp

The clamp seals the filter during all the important processes such as filtering, purging and drying. It was very important to have the clamp perform repeatedly well in each of these stages. Hence we dedicated a lot of time in trying to perfect the clamp design. In fact, although being successfully tested for contamination and preservation tests, the clamp is still being modified for improvements.

Compared to the previous design, the key changes of the new design are (i) A single

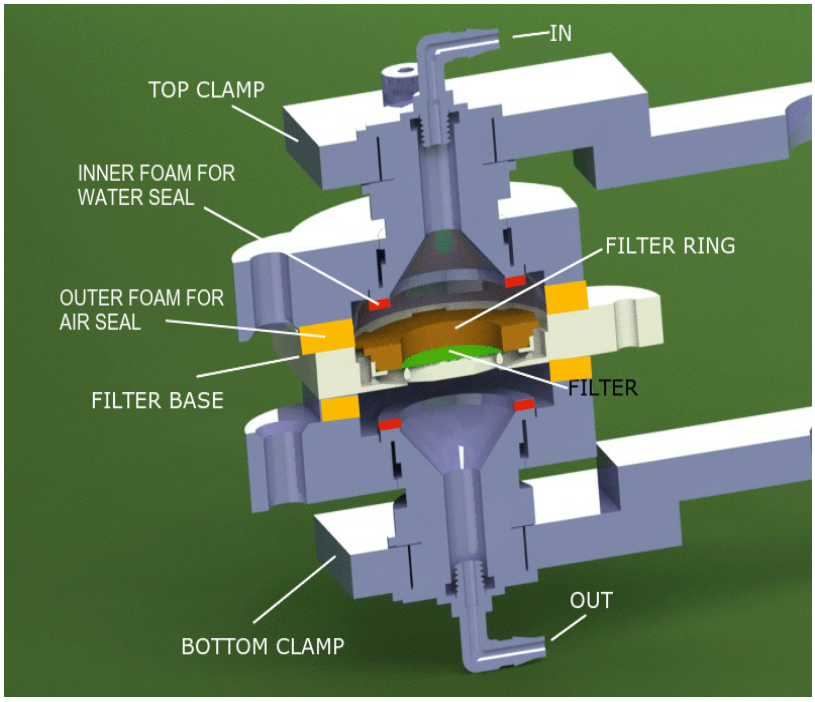

Figure 3.9: SolidWorks™ model - Cross section of the clamp setup around the filter

headed clamp design from a double headed clamp design (ii) 2-step clamp from a 1-step clamp; and (iii) 2 types of foam, one to achieve better compliance and the second one to prevent leakages. These design changes had impacts such as (i) faster initiation of the drying stage after filtering (improves preservation of sample), (ii) lesser space requirements and (iii) simplification of the control algorithm.

Fig. 3.9 shows a cross-section of the single headed clamp design. Also shown in Fig. 3.10 is the cross-section of the single-headed top clamp nozzle. Thus both water and air travels through the same head, unlike the previous double headed design. Reduction in size of the overall clamp is a direct impact of the new design. Also, the smaller clamp is a better option given the space constraints in the glider science-bay. Additionally, the single-headed clamp design provided us with the simplicity in controlling the positioning of the clamp.

Another important impact of such a design is that the drying process can be started immediately after filtering and purging is completed. The modification of having a 2-step clamp made this possible. This is an important functional requirement of the clamp. The drying process must be initiated as soon as the purging of water from the filter is completed.

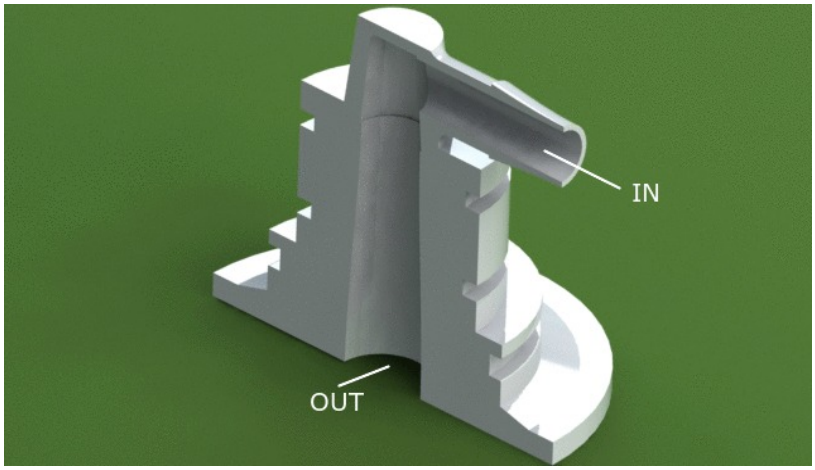

Figure 3.10: SolidWorks™ model - Cross section of top clamp nozzle

The biomass starts to denature if the filtered samples are not dried immediately after the purging stage. Hence, immediate drying of the filter is very important from the point of view of preservation of the sample in time.

The current clamp design features a two-step clamp. This can be seen in Fig. 3.9. The position of the clamp shown in the figure corresponds to the position required for drying process to be carried out. The outside seal is provided with the foam surrounding the filter. The second seal is the one in the center which directly rests on the filter ring once the clamp is in a compressed state. This seals the filter ring and thus prevents the filter from any leakages during the filtration process. Hence this two-step clamp ensures a seal both while filtering and during the drying stage without causing any restriction to the air flow.

3.3.5 Filter Bracket Design

Filter bracket design is one of the most important determining factors for successful filtration, purging and drying stages. Numerous designs were proposed and we started by testing if the design accomplished water filtration first.

Design with respect to filtration

In our prototype versions 1 & 2, the filter bracket was designed to support the filter against the pressure created by the water during filtration. This can be seen in Fig. 3.11. The filter would be placed on the metallic mesh and the sides of the filter were sealed using a nylon

ring, resting on the edge of the filter. This design however did not ensure the right pressure and hence, led the water to escape under the nylon ring instead of going through the filter. Therefore a redesign of the filter bracket was required to ensure proper seal around the filter.

Figure 3.11: A close up of the filter bracket for Prototypes 1 & 2

In order to achieve proper seal around the filter, the filter base design was modified as seen in the Fig. 3.12. The edge of the filter bracket has a small lip on which an O-ring sits that prevents any water leakage as well as holds the filter in place during filtration and drying. Fig. 3.12 shows the filter ring with a Buna-N O-ring that sits on the lip and seals the filter to help in proper filtration. Also to be noted are the notches that stick out from the circumference of this ring. The filter ring and the outer circumference of the filter slot leave gaps allowing the air to flow through during the drying process while keeping the filter in place. Fig. 3.12 shows how the ring sits on the lip of the filter bracket and the air gaps for air flow.

Design with respect to purging

After the filtration is completed it is important to purge the water since we do not want the water from the previous samples to remain in the water lines. The O-ring on top of the filter lip helps in purging the water through the filter.

The main reason to have a successful purge stage is that it has a direct impact on the drying stage. If the water is not purged effectively then it takes more time to dry. This

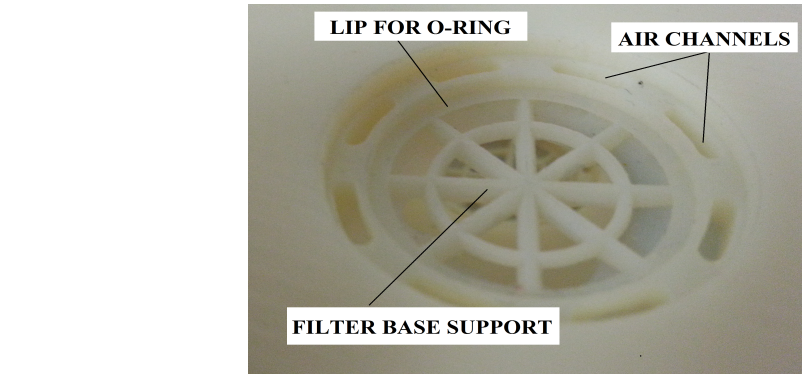

(a)

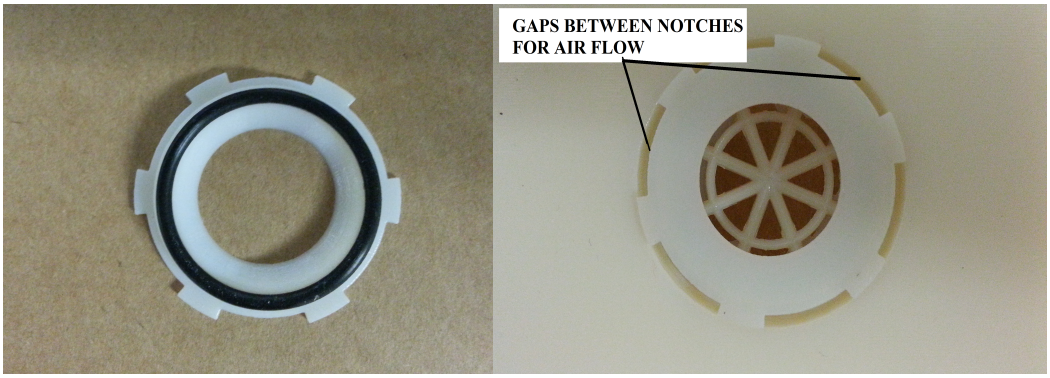

(b) (c)

Figure 3.12: (a) Current filter bracket design (b) Filter Ring with Buna-N O-ring (c) Filter ring sitting on the filter bracket

remaining water triggers the denaturing of the sample and render it useless for any biological analysis.

Design with respect to drying

As shown in Fig. 3.12, the air flows through the surrounding gaps drying the filter on top and then travels underneath to dry the bottom layer of the filter. Looking at the Solidworks™ model for the filter bracket shown in Fig. 3.13, it becomes clear how the air flows around and under the filter to dry it.

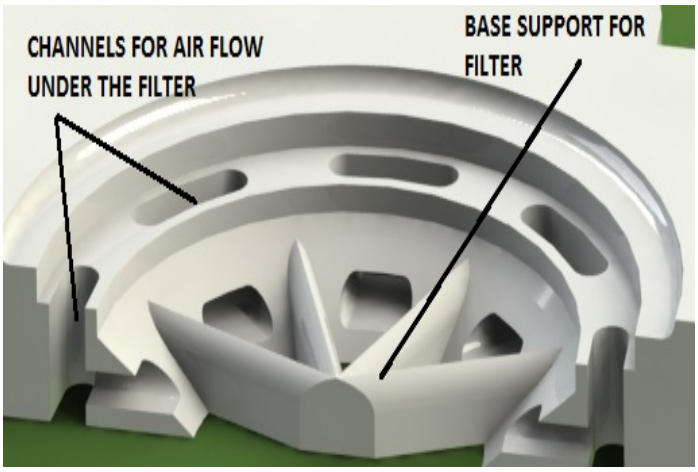

Figure 3.13: Solidworks™ model - Filter Bracket cross section showing the cavitites for the required air flow around the filter

3.3.6 Design evolution of the filter bracket

Avoiding the chain-reaction

One very important observation during the testing of the bio-sampler prototype was the consequence of the relationship between each of these processing stages of filtering, purging and drying and the way each one affected the other. If the first stage did not perform well, then the later stages will not be successful. Indeed all the three stages are related to each other and if one of them fails, then it creates a chain-reaction of failures for the other stages. For example, if the purging does not happen successfully, then lot of water will be trapped in the lines and on the filter. This would lead to a longer drying time indicating a defective drying stage. The filtered biomass will start to denature if the water stays on the filter for

a longer time. Hence, even a successful first stage of filtration, the entire sampling for that filter will be unsuccessful. This emphasizes the requirement of every stage to be completely successful every time.

Since the filter bracket design was a part of all the three stages, we reached the current filter bracket design after a number of design iterations as shown in Fig. 3.14. The difficulty in designing these filter brackets can be contributed to the fact that one small change in the design would effect all the three process stages.

These filter bracket designs were developed using Solidworks™. Once a design was developed, we used rapid prototyping techniques to test our designs within a small time frame. Since it was difficult to machine such precise and minute details, we took advantage of the 3D printing technology. This made the process of redesigning and testing extremely fast compared to traditional methods of machining. The reasons for each design change and their cross sections are also discussed in Fig. 3.14.

3.3.7 The "spitting" stage design

As understood from the several tests, for effective preservation of samples our most important tasks were, (i) to reduce the time gap between the filtration and drying stages and (ii) to purge majority of water before drying stage.

The latter problem was more important from the point of view of removing a major portion of water from the filter for two reasons. (i) The drying time will be longer if more water is retained on the filter and (ii) if water was left on the filter for a longer period of time, this situation would initiate enzymatic reactions to trigger the denaturing of biomass on the filter.

Working towards effective purging, we developed a technique of removing more water from areas around the filter. This technique, termed as "spitting", uses the air pump and the valves to create a sudden burst of air that forces out the trapped water and the water is "spitted" out. These trapped tiny water droplets did not get carried away even after the purging stage. Although the purging stage gets rid of 90 to 95 % of the water from the lines, filter, and the clamp, the final 5 to 10 % of water determines the drying time and hence the preservation of the biomass as discussed earlier.

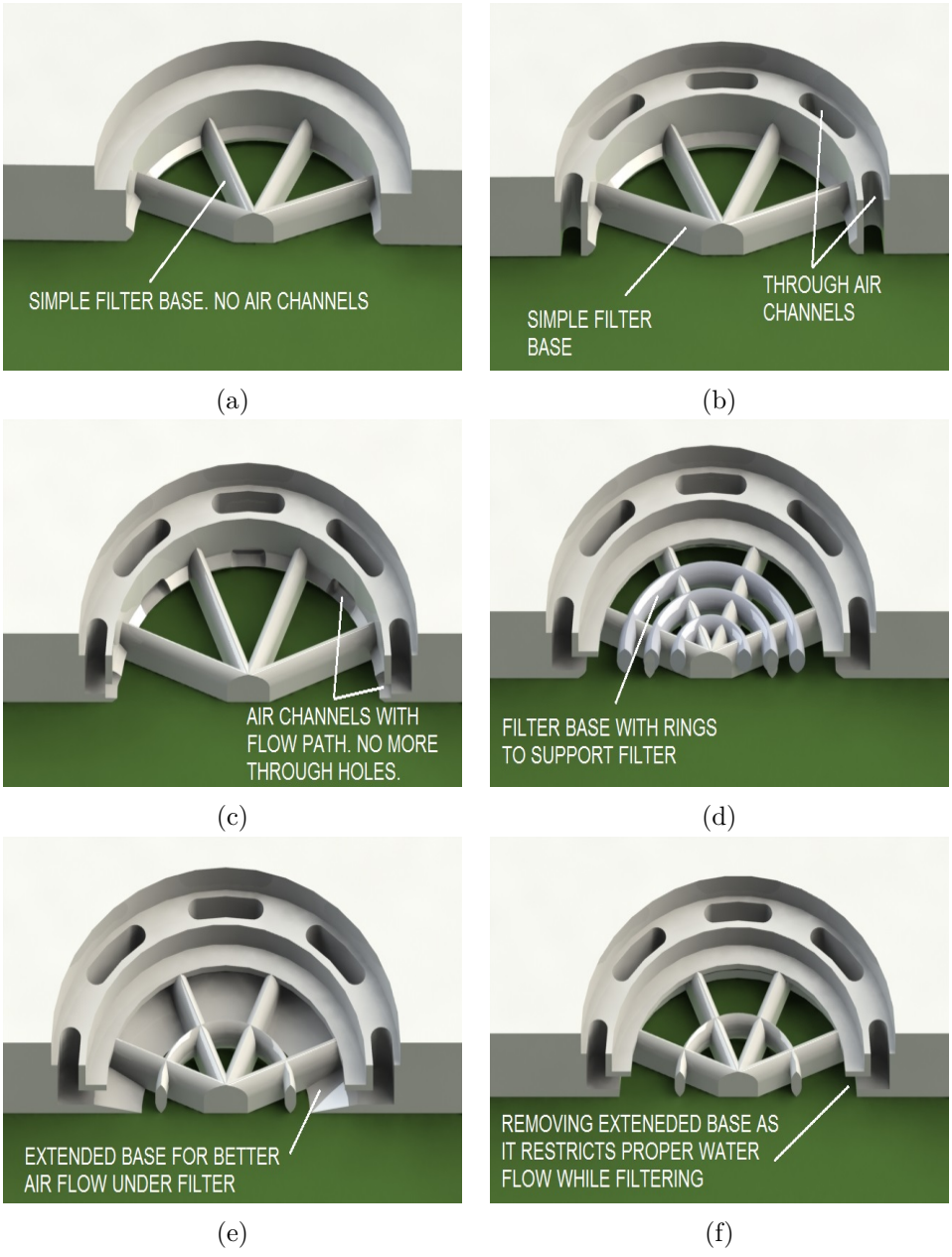

Figure 3.14: Evolution of the Filter Bracket designs. Each of these designs were repeatedly tested for filtering, purging and drying. (a) Filter Bracket having a simple support base for the filter and no air channels. Filtering and purging was good but not drying. (b) Introducing through air channels. The bottom part of the filter did not dry. (c) Air flow channels with flow paths to direct air under the filter. (d) Introducing support rings as base for filters since in some cases the filter cracked because of pressure after clogging. (e) Reducing the ring to just one as more rings trapped water while drying. Having extended air flow channels to improve in drying the bottom part of the filter. (f) Removing the extended base as it prevented water flow and increased internal pressure while filtering.

Principle of operation of the "spitting" stage:

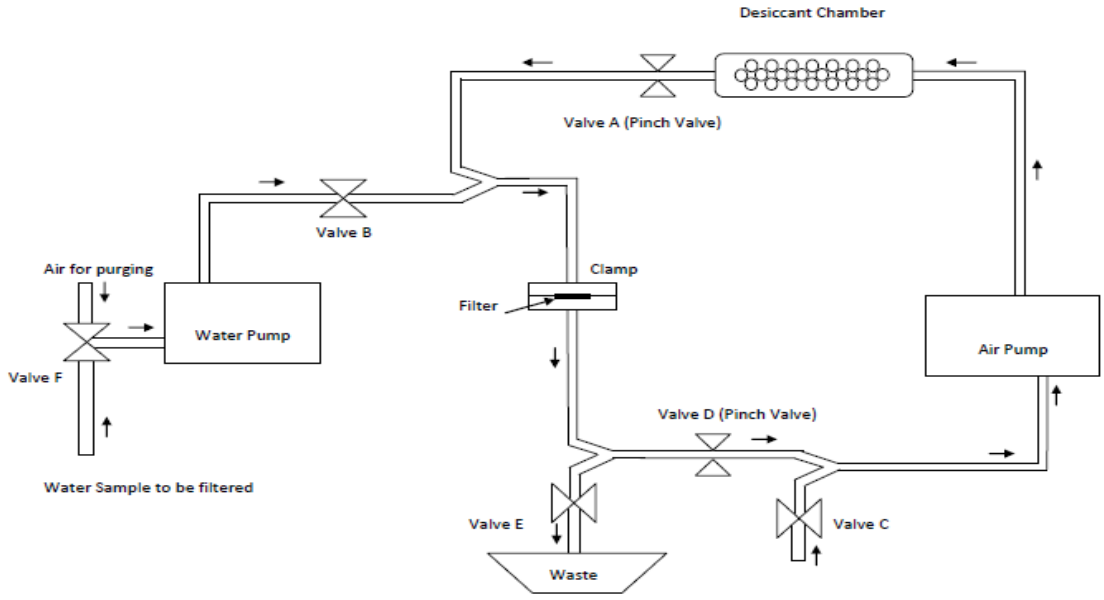

Figure 3.15: Tubing and valve setup showing the flow of air and water through the filter

As shown in Fig. 3.15 valve A in front of the desiccant chamber is used to spit the water out of the filter region.

Steps involved in the spitting stage

1. Purging complete.
2. Open clamp to remove the water seal but keeping the clamp air-sealed.
3. Open Pinch Valve A.
4. Start air pump (this helps in getting rid of some water due to air flow)
5. Close Valve A for few seconds then Open Valve A again ("spitting" of water due to increasing pressure and sudden release of air.)
6. The steps are repeated to have a chain of open and close commands for Valve A in order to attain multiple spitting incidents.

7. Close Valve C and E and open Pinch Valve D (this ensures a closed loop of air flow from the air pump and back to the pump via the desiccant chamber.)

8. In the closed loop stage "spitting" is continued again to force the remaining water, if any, out of the filter area.

3.4 Electrical Design

The overall schematic diagram of the current electrical system is shown in Fig. 3.16. The electrical design consists of the main Gumstix™ processor mounted on a RoboVero™ micro-controller. The three motors for each degree of freedom use Maxon™ 12 VDC motors which run through two SaberTooth™ motor control boards. One of the motor control boards can control 2 motors. The micro-controller has a dedicated UART port, configured to clock at 115.2 kbaud, which serves as a gateway between each of the motor control boards and the controller. A twisted pair shielded cable, grounded at the motor control board side, is also used to isolate the communication from any electrical noise. The use of the twisted pair cable is important since previous cases in which no such cables were used, had incidents of random motor jerks due to noise. Also, the use of power converters and solenoid valves in the circuit and their transient switching is a source of noise too.

Although the final glider-based bio-sampler is to be run on a battery pack, this bench top version was designed to be used with an AC to 24 VDC adapter which can be plugged into any regular wall AC supply. Also since this version is used in a lab and targeted to be used in the field, a simple plug-in adapter power supply was seen as the right option. The system also consists of DC-DC power converters since a lot of components do not run on 24 VDC. Hence, a 24V-12 VDC converter and a 24V-5 VDC converter were used in the design.

The entire relay board was designed based on proper power consumption calculations. Instead of the previously used 2A solid state relays, smaller IC solid state relays rated for 1A were used and these significantly reduced the footprint and the weight of the electrical system. A list of Digital Inputs (DIs) and Digital Outputs (DOs) used in our design are mentioned in Table 3.1. Since there were limited number of DIs and DOs, PWM pins 1

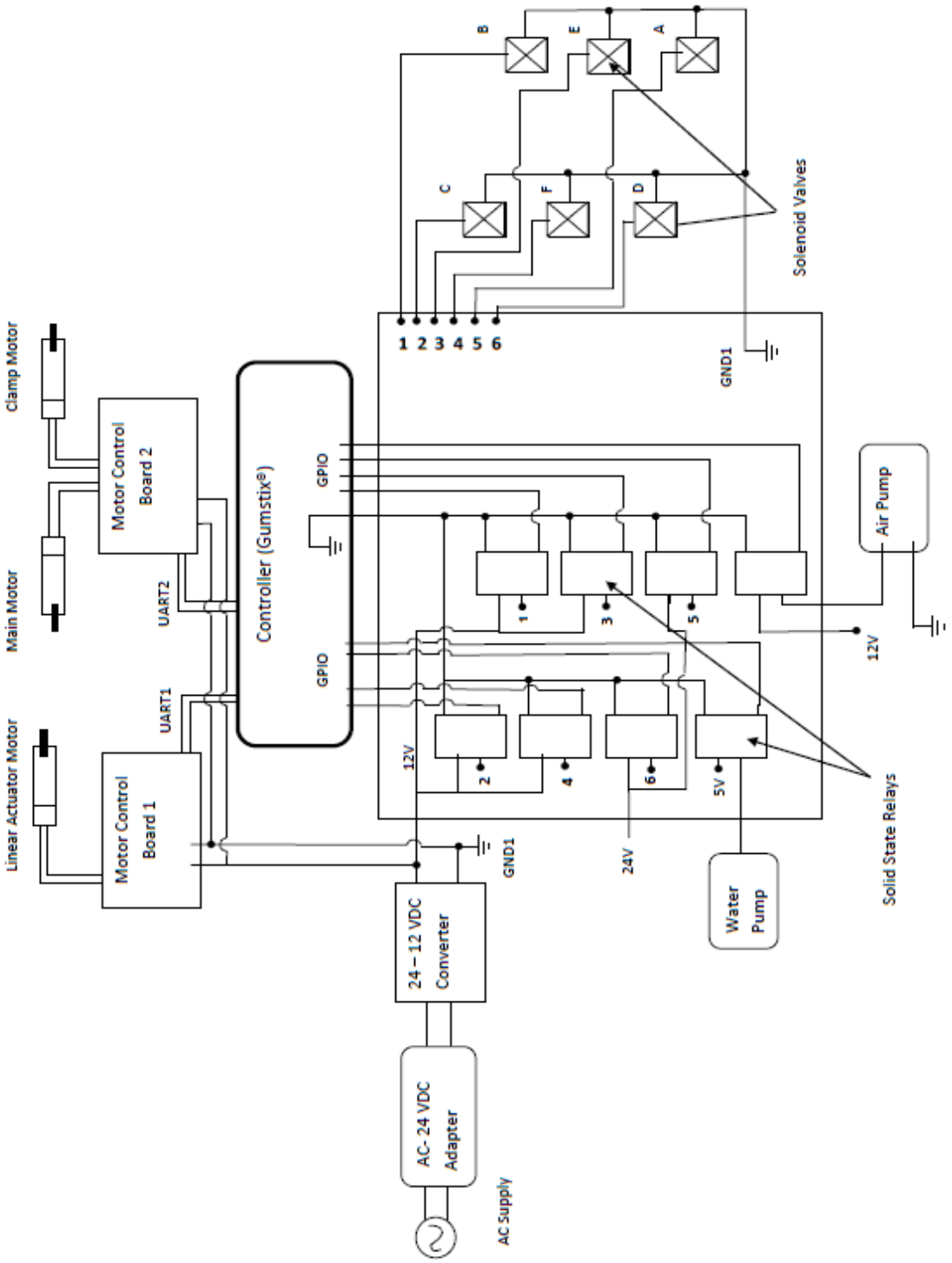

Figure 3.16: Current electrical schematic of the Biosampler

and 2 were also used as DOs. Limit switches were used for homing of all the three axes and also in positioning the filter with the clamp.

Table 3.1: List of Digital Inputs (DIs) and Digital Outputs (DOs) on microcontroller

DIs	Function	DOs	Function
P0_4	Filter positioning	P2_3	Valve D Open-Close
P0_5	Main motor Homing	P2_4	Valve A Open-Close
P0_20	Clamp Homing	P2_6	Valve C Open-Close
P1_27	Clamp close limit switch	P2_8	Water Pump On-Off
P4_28	Linear Actuator Homing	P2_10	Valve F Open-Close
P4_29	Filter Bracket Pos. 1	P0_19	Air Pump On-Off
		PWM 1	Valve B Open-Close
		PWM 2	Valve E Open-Close

3.4.1 Rotating Filter Bracket

The very first version of the rotating filter bracket had a central tube which would rotate with the help of a single DC motor and a gear box with torque ratio 1:139 at a full speed of about 30 rpm. It was difficult to estimate the torque of the motor initially since the parts were bound to changes in design. Hence, we assigned an upper limit and used a high torque motor of rating 10 kg-cm at 24 V. The rotation of the tube helps in aligning the filter with the clamp and in preventing the leakage of air and water. The tube also houses two SaberTooth ™ motor control boards for the main motor, the linear actuator motor, and the clamp motor. This is shown in Fig. 3.17. The central tube was first rotated to bring it to a home position using the limit switch feedback. This home position would serve as a reference for positioning the clamp with respective filter locations. Rest of the filter slot positions were reached by reading the encoder data and stopping at each filter by traversing a particular angle.

The current version of the central rotating shaft is comparatively simpler and is rotated using a geared DC motor with a gear ratio of 64:1. This motor is coupled to the motor shaft using a toothed belt instead of mounting it directly on the shaft of the motor unlike

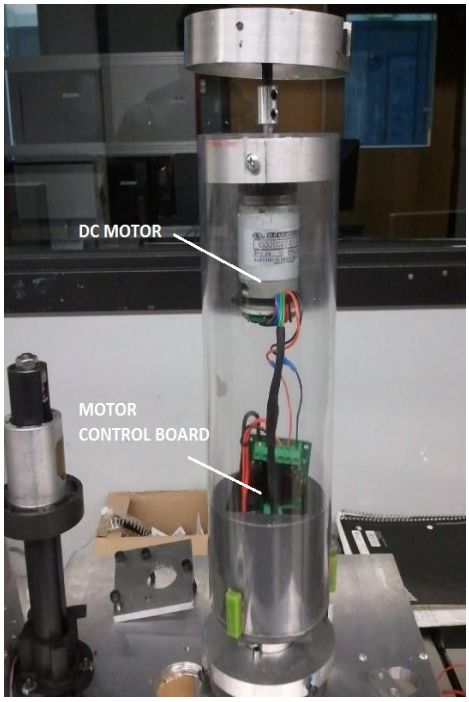

Figure 3.17: Rotating Filter Bracket housing for motor and motor control boards

the previous version.

3.4.2 The Linear Actuator

The linear actuator aligns the clamp with the filter brackets. The linear actuator is made up of a screw rail and a linear guide. The first version was actuated using a DC motor with a gear ratio of 1:172. Similar to the central tube, we used a high torque motor to compensate any misalignments in the linear actuator. Also, having a high torque meant lower speed which would help in achieving precise location of the filter brackets. The torque of this motor was 12.2 kg-cm at 12 V. The homing process of the linear actuator was similar to that of the central tube using a limit switch. The linear actuator would then reach each filter bracket using the encoder readings that were pre-determined after a calibration process.

The current version of the linear actuator however uses a less powerful DC motor and gear-head combination shown in Fig. 3.7. All the three motors that are used in the current version of the bio-sampler are exactly the same in terms of specifications. Each motor is a 12V Maxon™ DC motor with a gear ratio of 64:1. Calculations performed for torque

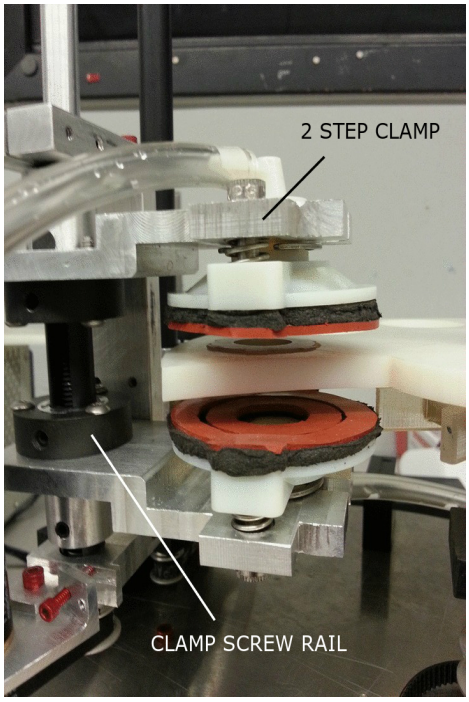

Figure 3.18: Current clamp design showing the 2 step clamp and the screw rail. At the bottom left corner is the toothed belt run by the DC motor.

requirements made it easy for us to decide these motors which had similar torque requirements.

3.4.3 Clamp Mechanism

The actuation for this mechanism in the first version was designed using a pneumatic system. The clamp would open and close using a pneumatic piston which was fixed on the linear actuator platform. The pneumatic system used a solenoid valve operated by the microcontroller which would control the time at which the valve was supposed to be opened or closed. However this mechanism was not successful. The flow of the water and air going into the clamp is controlled by the solenoid valves.

Current version of the bio-sampler as shown in Fig. 3.18 uses a DC motor with a gearbox for the clamp mechanism. The motor is controlled to take advantage of the 2 step clamp designed for efficiently filtering and drying of the water sample. The clamp is closed completely by running the DC motor until a limit switch sends a feedback indicating a proper

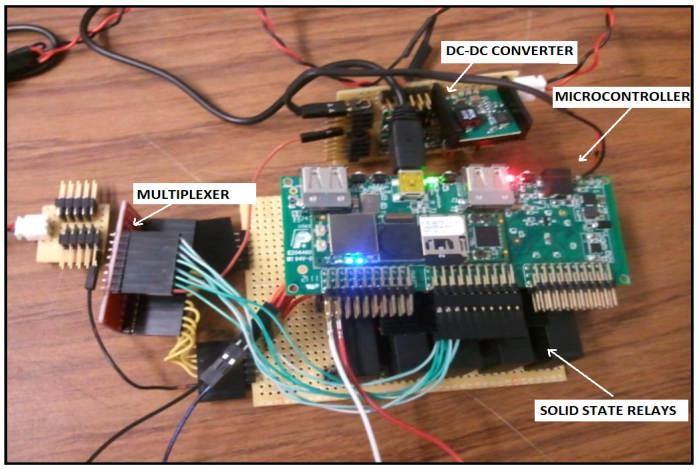

Figure 3.19: The entire circuit of prototype 1 showing the Gumstix™ ,relays and the power circuit

seal of the clamp around the filter. Once the filtering is completed, the DC motor starts to rotate in the reverse direction to open the clamp by 4mm to break the water seal but not the second seal outside to prevent air leakage. One advantage of the 2-step clamp as its ability to open and allow a far better air flow immediately after purging compared to the previous designs. Obtaining the home position of the clamp is also achieved using a limit switch.

3.4.4 Power Circuit

The entire bio-sampler system runs on 24VDC supply via an AC adapter. The other components like the DC motors, solenoid valves, water pump, etc., run on 12VDC. The encoders need 5VDC supply. Hence we made a small power circuit to regulate the incoming 24VDC supply to the required voltage levels.

3.4.5 Relay Circuit

We used solid state relays via the Gumstix™ to control and regulate the motor control boards, water pump, air pump, and the solenoid valves. The relays are able to handle output current up to 2A in the previous version. The relays used in the first version were heavy and occupied more space as shown in Fig. 3.19. Hence, for the current design we

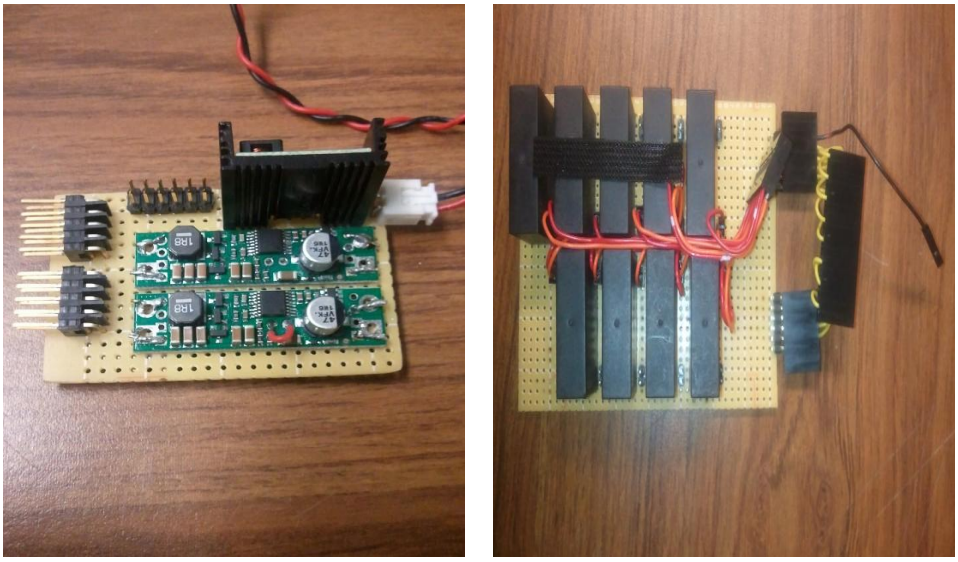

(a) (b)

Figure 3.20: (a) Power Circuit (b) Relay Circuit

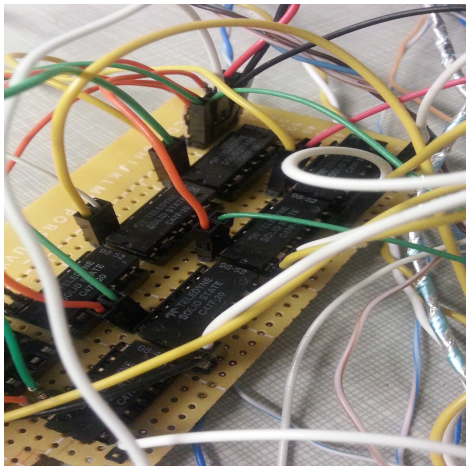

Figure 3.21: IC relays used in the current design

shifted to smaller Integrated Circuit (IC) relays that can handle currents up to 1A on the output side. Hence we planned to use the IC relays for low current consuming components like the solenoid valves and water pump. Larger relays were used for the motor control boards and air pump.

Fig. 3.19 shows the entire circuit including the Gumstix™ and RoboVero ™ . Underneath the controller is a set of relays and the power circuit is located on top. The motor control boards and the limit switches are mounted on the system in their respective locations.

3.4.6 PCB Design

The entire circuit were fabricated on a Printed Circuit Board(PCB), different from the perf-boards that were used before. The target was to have the electrical parts and the PCB board to be universal so as to be used till the final version of the bio-sampler. The relays are chosen as per the current requirements of each component so that we can reduce the size of the PCB board. Also, the power circuit and the Gumstix™ are all planned to be mounted on the same PCB board.

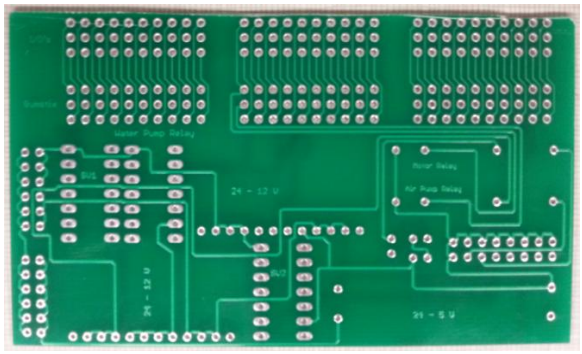

Figure 3.22: PCB Design

Changes in the circuit for the current design are being included in the new PCB design. This includes more solid state IC relays and different power converters since the number of valves and voltage ratings of the new pinch valves are different compared to the previous design of the electrical system.

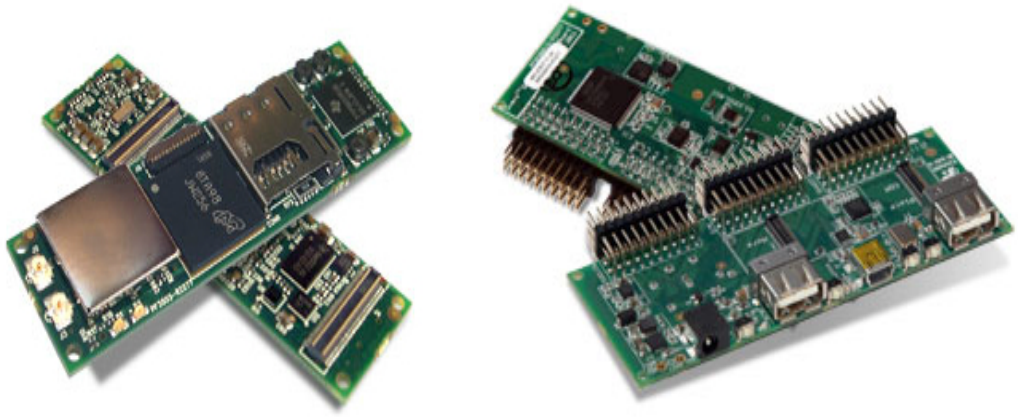

(a)

(b)

Figure 3.23: (a)Gumstix™ and (b) RoboVero™ micro-controller

3.5 Software Design

3.5.1 Gumstix™ Computer and RoboVero ™ micro-controller

The Gumstix™ Overo Air series is used for this prototype. It is an ARM Cortex-A8 OMAP3503 based computer-on-module. It is placed on the expansion board RoboVero ™ , a LPC1769 micro-controller board for robotics applications. Gumstix™ is an embedded Linux based system and uses Python script for coding. Gumstix™ has a good resource in the form of forums. The open source environment of the forum dicussion helped us choose the right library and boot files. We use serial Universal Asynchronous Receive Transmit (UART) commands to communicate with the motor control boards for speed control. The micro-controller has General Purpose Input Output (GPIO) that can be configured as inputs or outputs. The board communicates with a laptop/PC using a USB cable and can also be connected via 802.11g and Bluetooth. The Gumstix™ boots as soon as it is powered on and the user can interface with it via shell scripting.

We started initially considering Python as the main language due to the availability of Python libraries for the micro-controller. Since the libraries and example codes were available, it was straight-forward to start using the controller for our system. Python

was easy to use for our code development as it combines an intrinsically object oriented language with not too many unnecessary punctuations in simple function calls. Also the code was written in a "functional" form, where each function represented individual stages like filtering, purging, drying, etc. to look and function independently in the code as well. This structure made it easy to modify the code to use it for contamination test and the modify the same code to make the system completely autonomous. Also such a "functional" form of the code would make it easy for any programmer familiar with Python language to make modifications without having access to specialized compilers and other software development tools. The entire code modified for doing the contamination test II is given in Appendix A.

3.5.2 Bio-sampler program Design

The main program design modified for contamination test II consists of the procedure as follows.

1. **Initialization**: Set all outputs to low
2. **Get input from User**: Get user input for which filter location the clamp should be manipulated to
3. **Homing**: Start the sequence of homing
    - Homing clamp
    - Homing Central Disc
    - Homing Linear Actuator
4. **Manipulate**: Manipulate the clamp to the user defined filter location
5. **Choose an action**: After clamping at the required filter location, get user input to select what process is to be initiated out of the following:
    - Filter and Purge
    - Drying

- Filter, Purge, and Drying
- Priming

6. **Execute**: Start the chosen process
7. **Homing**: Go to home position again and wait for next user input, Go to Step 2

Chapter 4

Experimental Results

This chapter captures the experimental results obtained after testing the bio-sampler design. The samples collected from the bio-sampler are analyzed using standard processes such as gel electrophoresis and Terminal Restriction Fragment Length Polymorphism (TRFLP), carried out by marine scientists for analyzing macromolecules like DNA, RNA and proteins. The samples are tested for cross-contamination and preservation as a validation for the bio-sampler design.

4.1 Understanding the sample analysis techniques:

Sample extraction using gel electrophoresis:

The marine scientists use methods such as gel electrophoresis for separation and analysis of these macromolecules. It is a method of sorting molecules based on size using an electric field. The molecules move through an agarose gel under the influence of an electric field. Based on their size, some move faster while some move slower. These molecules form distinct bands on the gel. After the electrophoresis is completed, the molecules in the gel are stained to make them visible as shown in Fig. 4.1.

It is important for us to quantity these gel results in terms of quanitity and quality. If the bands are distinct it means that the macromolecules of that particular sample were intact. However, if the bands are smeared, then it means that the sample has degraded. Also darker bands refer to more quantity, lighter bands suggest that the process did not collect a lot of biomass or the sample started to degrade.

TRFLP profiling:

The process called Terminal Restriction Fragment Length Polymorphism (TRFLP) sample profiling is carried out as the next step in analyzing the collected samples. The profiles

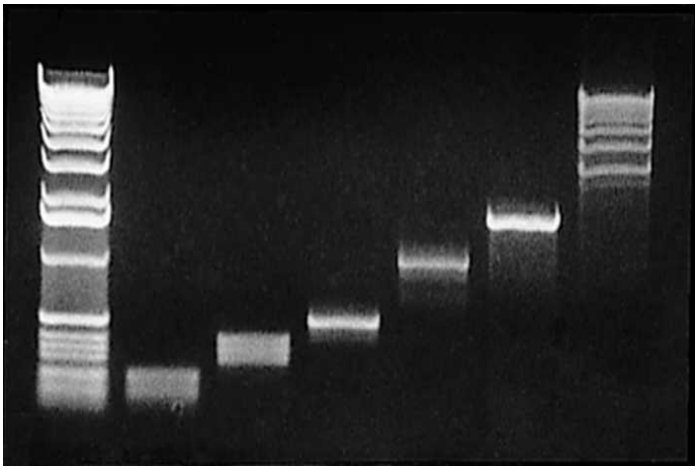

Figure 4.1: Gel-picture showing DNA fragments [11]

are created by amplifying the bacterial DNA from the extracts in the gel using a technology in biochemistry called the Polymerase Chain Reaction (PCR). The PCR is digested with a restriction enzyme and run on a genetic profiler. The restriction enzyme cuts the DNA into fragments that are different lengths, and the lengths are species dependent (i.e., different for each unique species in the sample). The x-axis is "fragment length", we call these Terminal Restriction Fragments (TRF) or Operational Taxonomic Units (OTU), and each fragment represents a single species. The y-axis is a measurement of fluorescence area units (the end of each fragment is fluorescently labeled during PCR), and this tells us the relative abundances of each fragment. In summary, x-axis is species diversity (each peak being a different species), and y-axis is relative abundance of each species. The TRFLP profile of sea water and river water used in one of our contamination tests is shown in Fig. 4.2. As we can understand, based on the location of these peaks along the x-axis, we can differentiate between sea water sample and river water sample. Hence, this serves as a very good tool in analyzing and comparing different samples.

The way to interpret a cross-contamination of samples using these profiles is by simply looking at peaks in both the profiles at the same point on the x-axis. If there are peaks overlapping between samples at the same point on x-axis, then it clearly indicates a cross-contamination between samples. If peaks are located at different locations along the x-axis in as seen in the figure, it suggests absence of cross-contamination and the sampling was

clean. Also, degradation of sample can be interpreted as comparing a reference sample with a sample under test. If the peaks of the test sample are smaller compared to the reference sample, it suggests that the sample has degraded.

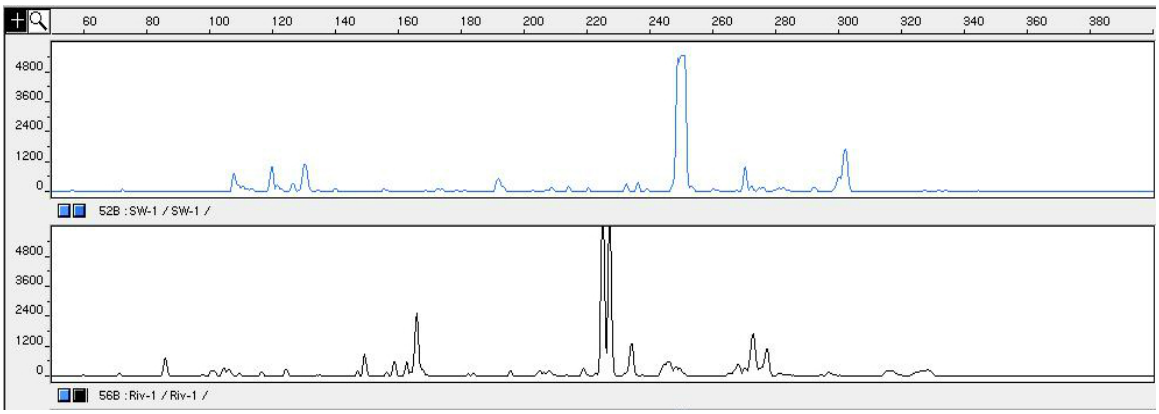

Figure 4.2: TRFLP profiles of sea water (top) and river water (below)

4.2 Contamination Tests I

We conducted sample contamination and preservation tests which serve as a yardstick to validate the design of the bio-sampler. These tests were conducted 'manually' only to test the 3D printed filter bracket and the single headed clamp mechanism and not the entire bio-sampler. Multiple filters were tested using two different water samples in the sequence described below to test for filtration of samples, cross-contamination and preservation.

The sequence of filtration was in the following manner:

1. Blank 1 - Clean Water
2. Sample A - Sea Water
3. Sample B - River Water
4. Sample A - Sea Water
5. Sample B - River Water
6. Blank 2 - Clean Water

The tests were conducted using sea water, and river water incubated over night with distinct organisms. Also clean sterile water was used as blanks to check for any remnants of previous sea or river water in the final clean water sample. We simulated the process of moving from one filter slot to the other using the sequence mentioned above. After the filtration was completed, the filters were immediately frozen in liquid nitrogen. The goal was to check for cross contamination between samples and also for the contamination in the blanks. We also collected samples of each water type manually, by standard procedures used by the marine scientists in the lab. These samples would serve as a reference sample called 'controls' to compare it with the test samples. Fig. 4.3 is the gel picture of these filters.

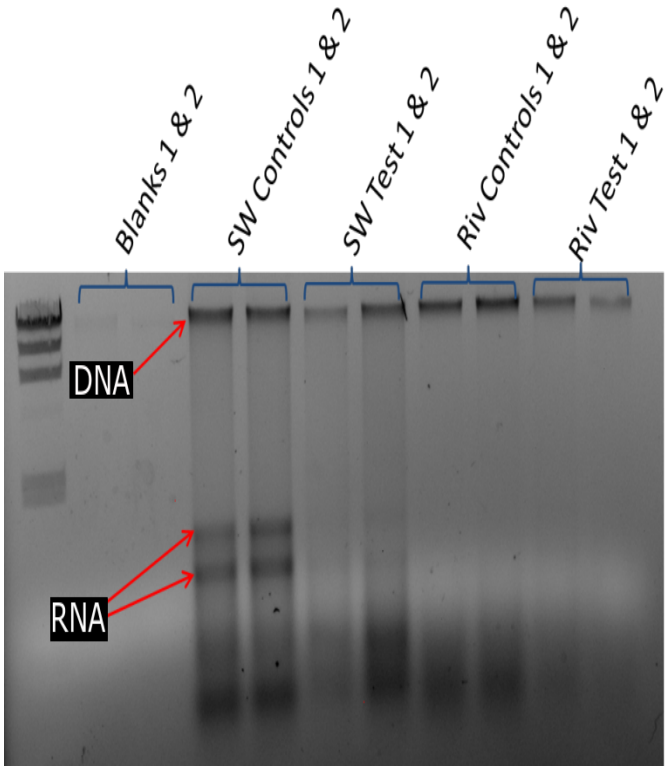

Figure 4.3: Results - Gel picture of Contamination Test I

The gel picture shows the quantity of the nucleic acids (DNA & RNA) in the controls and the extracts. In terms of the quantity of DNA in the sample, the intensity of the bands in (Sea Water) SW Test 1 & 2 and the (River Water) Riv Test 1 & 2 are lighter compared

to that of their respective controls. This indicates that the DNA of the test samples started to denature during the process. There were no RNA bands found in SW Test 1 & 2 but were present in their controls. This indicated that the RNA was completely degraded in the test sample. These results demanded more effective preservation of the test samples.

The time difference between the two stages (filtration and drying) and the long drying period was the reason for the degradation of the sample. Finally it was concluded that the level of degradation observed was not good enough to even proceed further in profiling the samples to check for contamination as the quantity of the molecules was not sufficient. Hence the first contamination tests were unsuccessful due to the reasons mentioned below.

We observed that the pump head and filter bracket were working well. However, the purging was not succesfull because of ineffective plumbing. Our hypothesis was that the filters remained too wet during the entire process and the 8-10 minutes necessary to dry the filters was also too long which resulted in denaturing of the sample. Majority of the water should be purged out of the filter within 10-20 seconds before the drying stage is initiated. However, approximately 50 micro-liters of water was retained on the filter prior to the drying step which aided in degradation of the sample. To reduce the time difference between the two stages (filtration and drying), the importance of having an automated version of this clamp set up was hence reinforced. Hence for the second contamination test we needed the system to be completely automated and redesigned to counter the limitations observed during contamination tests I.

Implications in design based on contamination tests I:

1. Reduction of time difference between the two stages (filtration and drying). A more important challenge is to get rid of water which is discussed below.

2. Design the system to purge majority of water autonomously. This step is critical to avoid any degradation observed in the contamination tests I.

3. Configuring the plumbing to fit the system around the filter. The plumbing will include number of valves, desiccant chamber, and drying pumps.

After the first contamination tests, our target was to eliminate all the faults that were

observed in the design and to improve the functioning of the whole system. The next step was to have an automated system to carry out the clamping since in the previous contamination test it was done manually.

4.3 Contamination Tests II

The current set up of the bio-sampler was used for performing the second set of contamination tests. This was done autonomously from the Bio-sampler as compared to the previous contamination tests which were done manually. The tests ran smoothly as we observed no leakages while filtering and this eliminated a major source of cross contamination of samples. The tests and the respective procedures are mentioned in the subsections below.

4.3.1 Contamination Tests

The second set of contamination tests were done in which the samples were filtered, purged and immediately frozen. Each sample was performed with a priming stage in which the water supposed to be filtered was run through the whole system before filtering so as to clear any remains of previous sample water.

The sequence of filtration was similar to the first contamination tests in the following manner:

1. Blank 1 - Clean Water
2. Sample A - Sea Water
3. Sample B - River Water
4. Sample A - Sea Water
5. Sample B - River Water
6. Blank 2 - Clean Water

This would give us a status of cross contamination in between samples by following the above sequence of Sample A, Sample B, Sample A, Sample B. The 2 blanks would give us

if after these filtration any of the two Samples A or B, show up as contaminants while we filter out clean water on Blank 2.

4.3.2 Preservation Tests

We also completed the preservation tests by drying the sample from our system and not freezing it as done in the contamination tests. These tests validate the bio-sampler's drying stage. If the preservation of biomass is found to be good, that confirms the working of drying stage to be as required.

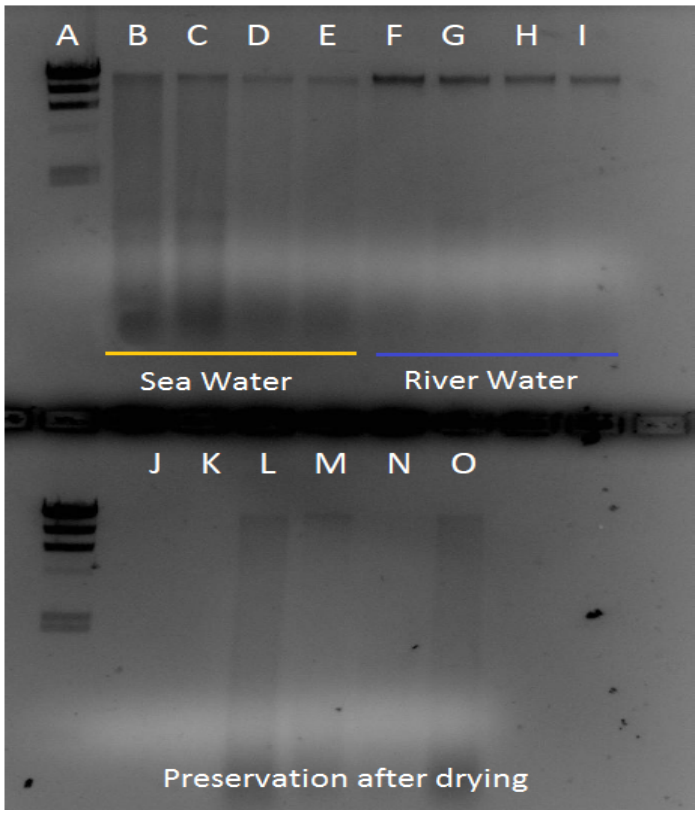

Figure 4.4: Results - Gel picture of Contamination Test II

Preservation tests were done in two different scenarios:

1. Drying for 10 mins
2. Drying for 15 mins

This is to verify if preservation is directly related to the time that we dry the sample for. We are also interested in finding out if the rate of drying affects the preservation. That is to test the affect of how quickly we are able to dry the major portion of water after filtration so that we prevent any biological activity on the filter that could denature our collected samples.

The key for understanding the Fig. 4.4 is given in Table 4.1.

Table 4.1: Key for the gel picture

	A - Size standard (Reference)	B - Sea water Control 1
	C - Sea water Control 2	D - Sea water Contamination Test 1
	E - Sea water Contamination Test 2	F - River water Control 1
	G - River water Control 2	H - River water Contamination Test 1
	I - River water Contamination Test 2	J - Contamination Blank 1
	K - Contamination Blank 2	L - 10 min Preservation Test 1
	M - 10 min Preservation Test 2	N - 15 min Preservation Test
	O - No O-ring test Preservation Test	

The contamination and preservation test results are shown in Fig. 4.4. Also important to note is that the RNA bands are not visible in these gel pictures because of the way the samples were prepared. Hence even the control samples do not show any RNA bands for comparison. However, this would still let us consider the sampling and test results to be valid by comparing and analyzing the DNA material alone. Let us consider the results both in terms of preservation and contamination.

Validation of the Bio-sampler for preservation

The preservation of the sample was done by the process of drying the filters for 10 minutes. As seen in the gel picture, columns L, M, N and O show the preservation results. These tests were done using only sea water. As we can see clearly, there is some amount of DNA in the gel picture in columns L, M and O. This confirms that the system was able to preserve the sample although there was a little loss as compared to the controls. Column N was for a sample which was dried for 15 minutes and it was to verify if drying for a longer duration had any effect on preservation. However, it does not show significant amount of

genetic material in the gel picture.

As pointed out earlier these samples were not frozen at all. They were dried by the sampler and simply stored away in small filter tubes at room temperature. They were analyzed for preservation after being stored in these tubes for 10 days. These results confirm that the sampler was able to do the preservation of samples as well but with certain amount of loss which could be improved upon based on design modifications.

Validation of the Bio-sampler for contamination

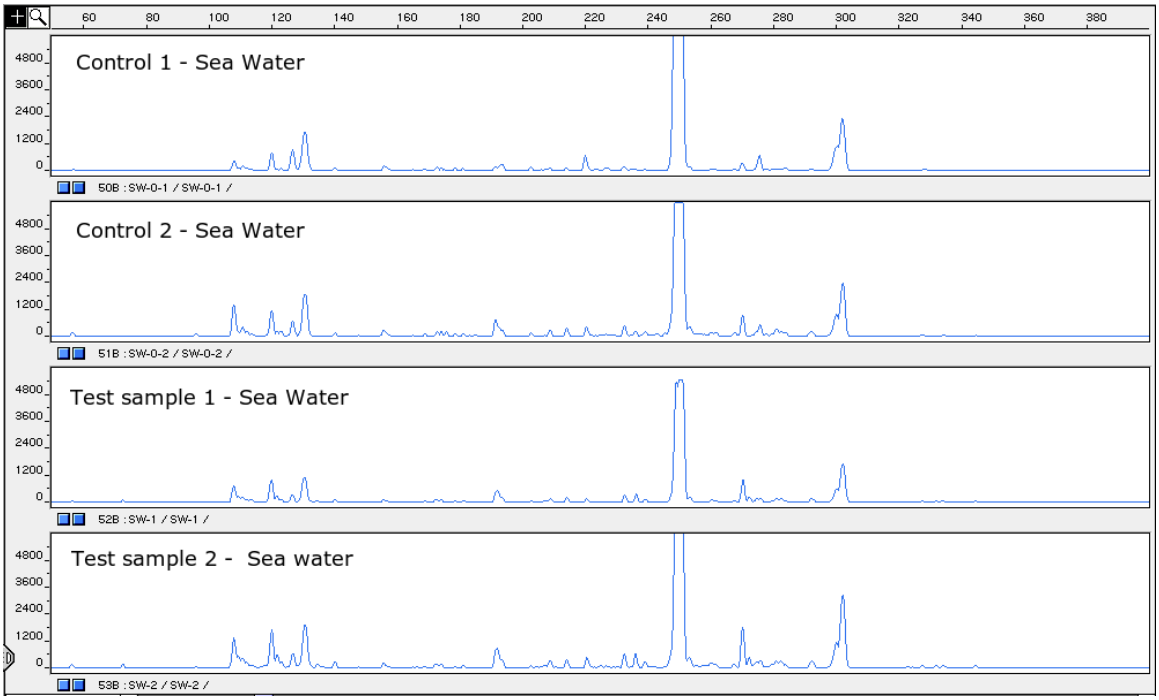

Figure 4.5: TRFLP profiles for sea water - Controls and test sample from bio-sampler

Let us consider the Fig. 4.4, the two contamination blanks 1 and 2 depicted by column J and K respectively. The blank J was taken right before we started the sampling process. The second blank K was taken right after we completed our sampling process as described in the sequence. The purpose of these blanks was that both should look similar to each other. The reason behind it being that if during the sampling process any of the water samples are contaminating the next sample by being carried over by the clamp, then there should be some biomass seen in blank K. However as seen from the gel picture, no quantity of DNA or RNA was registered on the filter blanks 1 and 2 shown by columns J and K.

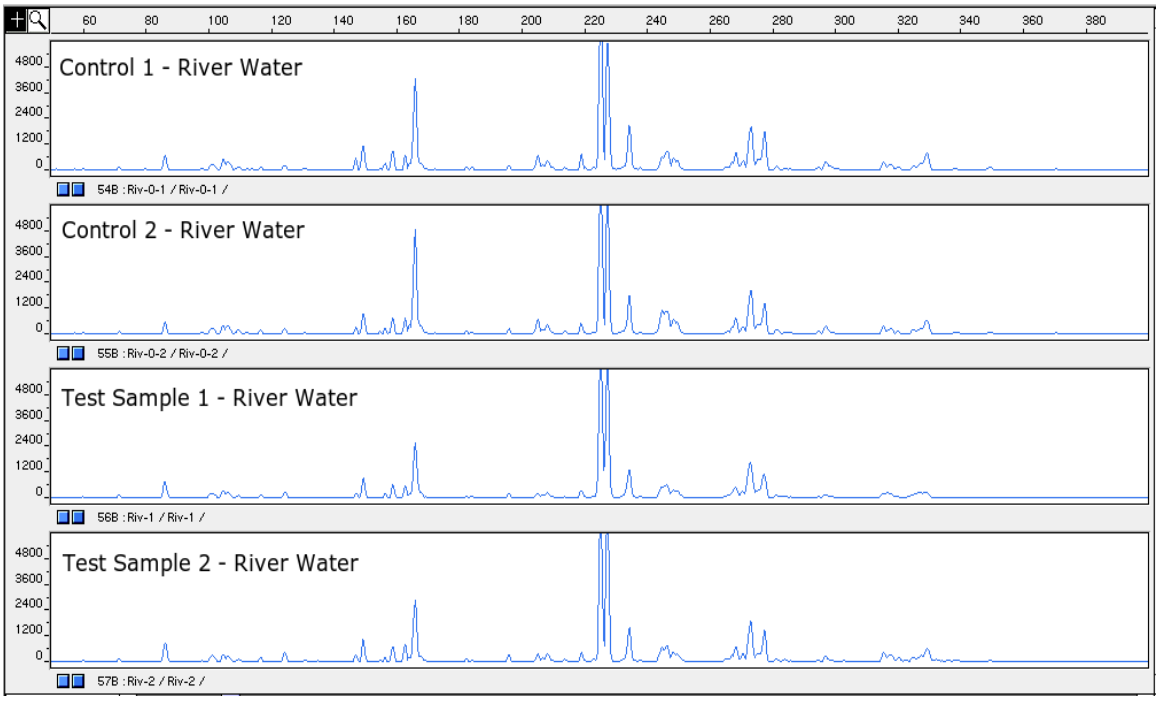

Figure 4.6: TRFLP profiles for river water - Controls and test sample from bio-sampler

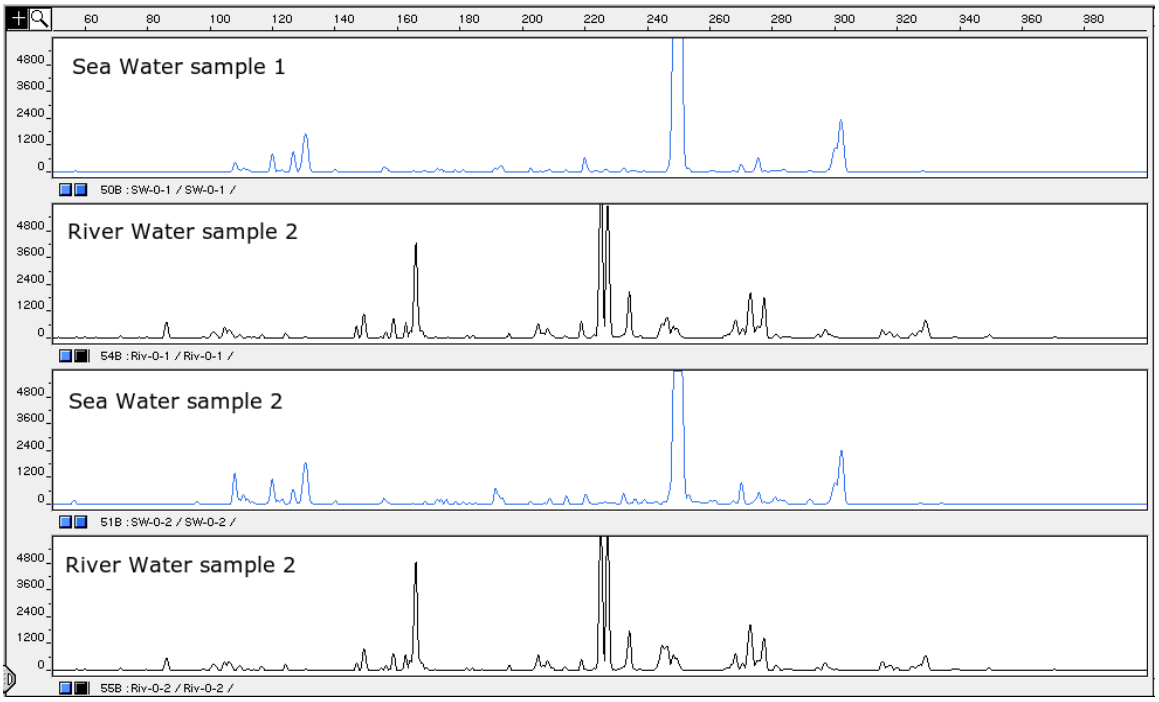

Figure 4.7: TRFLP profiles confirming no cross-contamination between samples - Test samples for sea water and river water

This confirms that the bio-sampler does not contaminate into the blanks.

This result is further strengthened from the TRFLP profiles that were generated for these contamination tests. As seen in Fig. 4.5 and Fig. 4.6, it is clear that the bio-sampler was able to perform effective filtration. The profiles of filtered sea water and river water were found to be very similar to their respective control samples. Fig. 4.7 shows the profiles for both sea water and river water. There are no peaks in common between these two sample which confirms that the bio-sampler did not cause any cross-contamination between samples during the tests. These results confirm a successful automated sampling and contamination test.

4.4 Current status

As seen from the results the bio-sampler was able to carry out successfully sampling without any cross-contamination. The bio-sampler was also able to preserve bio-mass which was analyzed 10 days later.

However, there was degradation observed in the preserved sample after 10 days compared with that of the control sample on day 1. This duration of preserving the sample needs to be improved more since the gliders are generally deployed for weeks or even months before they are retrieved after a mission. Hence, to further improve the preservation achieved using the drying stage, currently the biosampler is undergoing modifications in the filter bracket design and in the clamp design.

The problem:

As seen in Fig. 3.12, the purpose of the filter ring sitting on top of the filter to seal the filter and facilitate the water to go only through the filter. This is good design from the perspective of having a good filtration and purge through the filter. However, this design prevents a proper air flow around the filter since it traps water close to the rubber O-ring which is still sitting on top of the filter while drying.

The Solution (A "floating" filter):

One way to prevent this is to have the filter ring fixed on the inside of the upper clamp. This will seal the filter while the clamp is in the closed position and help filtration to go

through as desired. Also while we open the clamp slightly before the drying stage is started, it will break that seal and help in better air flow around the filter as the filter ring is no longer sitting on the filter. This design will also help to force the water away from the filter as soon as possible. This would be possible in the absence of the seal and the filter would simply "float" and flutter in the filter slot within the clamp, while there is a good air flow around the filter. This would further help in reducing the drying time of the filter and improve the preservation of the biomass as we try to get rid of the water as quickly as possible.

This design change would require us to modify the upper clamp and the 3D printed filter bracket. Currently design changes are being made in both components in order to test out our solution.

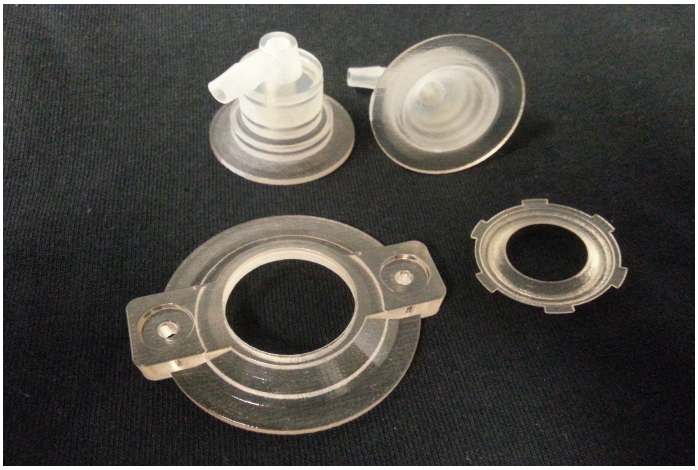

Figure 4.8: Contamination Test Results

Also as shown in the figure above, we have printed out the clamp parts in clear plastic material. This would be used with colored water in order to actually see how the water flows through the filter. This procedure would also give us a view of how and where the water might be getting trapped during the drying process. It would help us understand our design better and also help us in making modifications to improve the drying process further in terms of sample preservation.

Chapter 5

Localization in underwater glider used model-based approach

This chapter constitutes the second part of this thesis. In this chapter, we present a dynamic model-based localization algorithm to improve the positioning estimation of the Slocum glider because there are limited number of positioning sensors on-board the glider. This localization approach is built on an experimentally validated glider dynamic model and fused with on-board sensor measurements such as the depth and the yaw angles. Also comparison of our localization scheme with the previous glider flights equipped with Doppler Velocity Log (DVL) sensors and Dead Reckoning method is also shown in this chapter.

5.1 The rationale behind our localization scheme

The rationale behind the proposed approach is straightforward: if we can precisely capture the motion dynamics of glider navigation, with the known inputs to the glider, the dynamic model should be able to predict its positioning and motion information. A fusion of the glider dynamic model and the measurements of the on-board sensors can further improve the positioning estimation. In line with this thought we used an Extended Kalman Filter (EKF) to integrate the dynamic model with the depth and pitch angle measurements [20]. The validation of our scheme is done from the experimental data from previous glider deployments that were carried out by the Rutgers University Coastal and Ocean Observation Lab (RUCOOL) [12]. The results confirm the improvement in performance caused by the new positioning scheme as opposed to the commonly used dead reckoning method. The dynamic model is based on the one in [13]. But in our model we provide a different and simple derivation through Lagrange's equations. Moreover, our model is also valiated by the experimental data of previous glider deployments which were obtained from the RUCOOL Lab. In this work we are validating the dynamic model by experimental data.

5.2 Slocum Glider Dynamic Models

5.2.1 Slocum Gliders

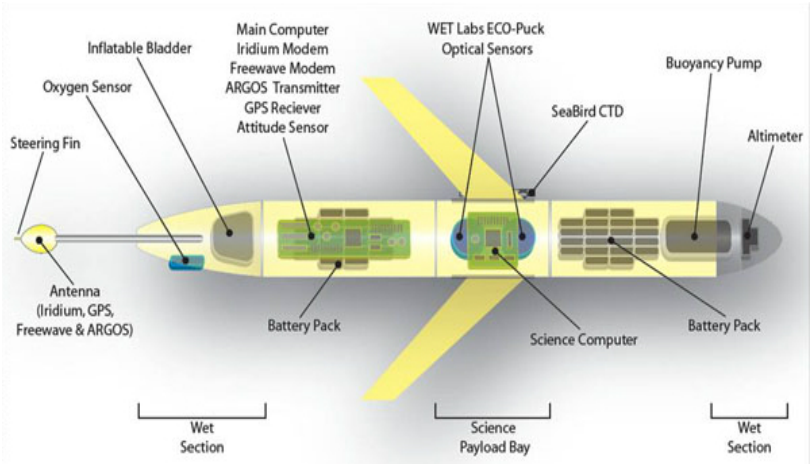

Figure 5.1: Structure of Slocum Glider [19]

Fig. 5.1 shows the structure of the Slocum [19] gliders made by Webb Research Corporation. The glider consists of three main sections. The front part mainly contains the buoyancy engine, including the water pump and the motor-actuated mechanism. This mechanism is to move and rotate the battery pack. The underwater navigation is built on dead reckoning algorithms with on-board sensors such as the altimeter and the attitude sensor that provides bearing, pitch, and roll angles. The middle part of the glider is the science bay, mainly containing the scientific sensors and instruments like on board sensor suites. The rear portion contains the glider control boards (i.e., flight controller), tail-fin and the rudder. Communication antenna (for GPS and satellite telecommunication) is built inside the tail-fin as shown in Fig. 5.1. An air bladder is also installed inside the rear cowling for emergency floating. Two side fins are mounted on outside of the science bay. These fixed fins are not actuated. The heading (yaw) motion of the glider is actuated through the rudder control and the battery pack rotation. The glider movement is primarily actuated by the varying the ballast water mass through the buoyancy pump and the slow movement of battery position. The glider floats to sea surface periodically (i.e., several hours), localizes itself through GPS and receives commands for the next navigation way-points. The

glider's motion control, navigation algorithms, and data collections are all implemented on the control board [20].

5.2.2 Kinematic Relationships

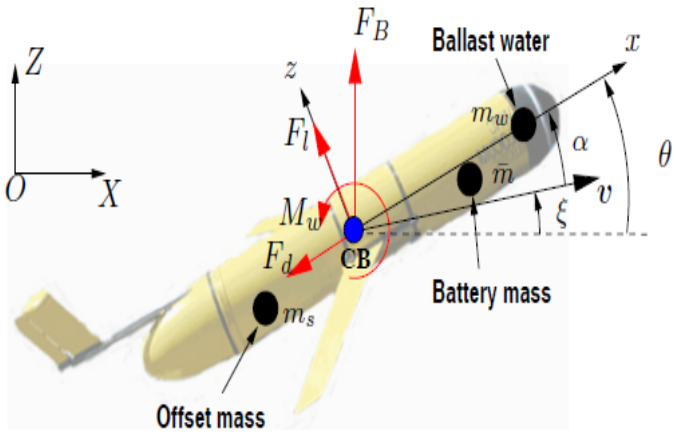

Figure 5.2: Motion and force schematic of Slocum gliders (the gravitational forces for each part are not explicitly shown.) [20]

Fig. 5.2 shows the schematic of the motion and forces for the Slocum autonomous glider. We assume that the glider's motion is restricted only in the vertical plane. Two coordinate systems are used in the model derivation: the ground-fixed inertial frame $\mathcal{I}_E$ with unit vectors $(\mathbf{I}, \mathbf{K})$ along the X- and Z-axes, respectively, and the glider body-fixed frame $\mathcal{I}_B$ with unit vectors $(\mathbf{i}, \mathbf{k})$ along the x- and z-axes, respectively. The origin of $\mathcal{I}_B$ is located at the buoyancy center (CB). We consider the glider system that consists of four masses: the hull mass with center at CB, the offset mass, the battery mass, and the ballast water mass; (see Fig. 5.2)

We denote the CB location at $\mathbf{r_{CB}} = \mathbf{xI}+\mathbf{zK}$ in $\mathcal{I}_E$. We also denote the position vectors of the offset mass, the sliding battery mass, and the ballast water mass in $\mathcal{I}_B$ as

$$\mathbf{r_i^s} = \mathbf{r_{ix}i} + \mathbf{r_{iz}k},\ \mathbf{i} = \mathbf{s}, \mathbf{p}, \mathbf{w}, \tag{5.1}$$

where the subscripts $i = s, p, w$ represents for offset mass, battery mass and ballast water mass, respectively. Then the absolute position vectors in $\mathcal{I}_E$ for the offset mass, the

battery mass and the ballast water mass are respectively as shown below

$$\mathbf{r_i} = \mathbf{x_i}\mathbf{I} + \mathbf{z_i}\mathbf{K} = (\mathbf{x} + \bar{\mathbf{x}}_\mathbf{i})\mathbf{I} + (\mathbf{z} + \bar{\mathbf{z}}_\mathbf{i})\mathbf{K},\ \mathbf{i} = \mathbf{s}, \mathbf{p}, \mathbf{w}, \tag{5.2}$$

where $x_i = x + \bar{x}_i$, $z_i = z + \bar{z}_i$, and the relative positions

$$\bar{x}_i = r_{ix}c_\theta - r_{iz}s_\theta,\ \bar{z}_i = r_{iz}c_\theta + r_{ix}s_\theta, \tag{5.3}$$

where notations $c_\theta := \cos\theta$ and $s_\theta := \sin\theta$ for θ and other angles. We also use the rotational relationship between vectors $(\mathbf{I}, \mathbf{K})$ and $(\mathbf{i}, \mathbf{k})$ through angle θ in (5.2). Therefore, it is straightforward to obtain the velocity vectors for the offset mass, the battery mass, and the ballast water mass:

$$\begin{aligned} \mathbf{v_i} &= \dot{\mathbf{r}}_i = \left[\dot{x} + \dot{r}_{ix}c_\theta + (-r_{iz}c_\theta - r_{ix}s_\theta)\,\dot{\theta}\right]\mathbf{I} + \\ &\quad \left[\dot{z} + \dot{r}_{ix}s_\theta + (r_{ix}c_\theta - r_{iz}s_\theta)\,\dot{\theta}\right]\mathbf{K},\ \mathbf{i} = \mathbf{s}, \mathbf{p}, \mathbf{w}. \end{aligned} \tag{5.4}$$

5.2.3 Calculation of the hydrodynamic forces

The glider's velocity vector $\mathbf{v_{CB}} = \dot{\mathbf{r}}_\mathbf{CB} = \dot{\mathbf{x}}\mathbf{I} + \dot{\mathbf{z}}\mathbf{K} = \mathbf{v_x}\mathbf{i} + \mathbf{v_z}\mathbf{k}$, where v_x and v_z are the velocities along the x- and z-axis in $\mathcal{I}_B$, respectively. The glider's path angle ξ and attack angle α are calculated as

$$\xi = \arctan 2\,(\dot{z}, \dot{x})\ \ and\ \ \alpha = \arctan 2\,(v_z, v_x)\,, \tag{5.5}$$

respectively. From Fig. 5.2, we obtain

$$\alpha = \theta - \xi. \tag{5.6}$$

The calculations of the hydrodynamic forces F_l, F_d and torque M_w are as follows.

$$F_l = \frac{\rho A v_r^2}{2} K_L |s_{2\alpha}|,\ F_d = \frac{\rho A v_r^2}{2}\left(K_{D0} + K_{D1}\alpha^2\right), \tag{5.7}$$

$$M_w = \frac{1}{2}\rho A v_r^2 K_{R1}\alpha - K_{R2}\dot{\theta}. \tag{5.8}$$

The buoyancy force $F_b = \rho g V$. In above equations, the term $\frac{1}{2}\rho A v_r^2$ is the dynamic pressure and the relative velocity v_r is $v_r = \|\mathbf{v_r}\|_\mathbf{2} = \sqrt{(\mathbf{v_{CB}} - \mathbf{v_c})^\mathbf{T}(\mathbf{v_{CB}} - \mathbf{v_c})}$, where $\mathbf{v_c}$

is the ocean current velocity vector. In this work, we assume that the zero ocean current velocity, i.e., $\mathbf{v_c} = \mathbf{0}$.

Considering the asymmetrical structure of the glider along the z-axis, the values of hydrodynamic parameters K_L, K_{D1} and K_{R1} are different for positive and negative sign of angle α. If $\alpha > 0$, constants K_L^+, K_{D1}^+, and K_{R1}^+ are used for K_L, K_{D1} and K_{R1}, respectively; instead, we use constants K_L^-, K_{D1}^-, and K_{R1}^-, respectively. For M_w calculation in (5.8), the first term is effective under steady motions, while the second term is used to capture the pitching resistance given by ocean water [20].

5.2.4 Dynamic models

We take Lagrange's equations to derive the glider motion equations. The glider is under control of the sliding battery's position r_{px} along the x-axis in $\mathcal{I}_B$ and the varying ballast water mass m_w. We define the generalized coordinate $\mathbf{q} = [\mathbf{x}\ \mathbf{z}\ \theta\ \mathbf{r_{px}}]^{\mathbf{T}}$ and the total mass $m_T = m_h + m_p + m_s + m_w$. The Lagrangian $\mathcal{L}$ of the glider is the same as the total kinetic energy, namely,

$$\begin{aligned}\mathcal{L} &= \frac{1}{2}m_h\mathbf{v_{CB}}\cdot\mathbf{v_{CB}} + \frac{\mathbf{1}}{\mathbf{2}}\mathbf{m_p}\mathbf{v_p}\cdot\mathbf{v_p} + \frac{\mathbf{1}}{\mathbf{2}}\mathbf{m_w}\mathbf{v_w}\cdot\mathbf{v_w} + \\ &\quad \frac{1}{2}m_s\mathbf{v_s}\cdot\mathbf{v_s} + \frac{\mathbf{1}}{\mathbf{2}}\mathbf{J}\dot{\theta}^{\mathbf{2}}.\end{aligned}$$

The total virtual work δW is obtained as

$$\begin{aligned}\delta W &= u_r\delta r_{px} - m_h g\delta z - m_p g\left(\delta z + \bar{x}_p\delta\theta + \delta r_{px}s_\theta\right) - m_s g \\ &\quad \left(\delta z + \bar{x}_s\delta\theta\right) - m_w g\left(\delta z + \bar{x}_w\delta\theta\right) + F_b\delta z - F_d c_\xi\delta x \\ &\quad -F_d s_\xi\delta z - F_l sign(\alpha)s_\xi\delta x + F_l sign(\alpha)c_\xi\delta z + \\ &\quad M_w\delta\theta + K_{R2}\dot{\theta}\delta\theta,\end{aligned}$$

where $sign(\alpha) = 1$ if $\alpha \geq 0$ and -1; otherwise. The generalized forces are then obtained

$$F_1 = -F_d c_\xi - F_l sign(\alpha)s_\xi,$$

$$F_2 = -F_d s_\xi + F_l sign(\alpha)c_\xi - m_T g + F_b,$$

$$F_3 = -\textstyle\sum_{i=p,s,w} m_i\bar{x}_i g - K_{R2}\dot{\theta},\ F_4 = u_r - m_p g s_\theta,$$

where u_r is the motor force applied to the battery pack. Considering the form of Lagrange's equations

$$\frac{d}{dt}\left(\frac{\partial \mathcal{L}}{\partial \dot{q}_k}\right) - \frac{\partial \mathcal{L}}{\partial q_k} = F_k,\ k = 1, 2, 3, 4,$$

we obtain

$$\mathbf{M}(\mathbf{q}, \mathbf{u})\ddot{\mathbf{q}} + \mathbf{C}(\mathbf{q}, \dot{\mathbf{q}}, \mathbf{u}, \dot{\mathbf{u}}) + \mathbf{G}(\mathbf{q}, \mathbf{u}) = \mathbf{u_r}, \tag{5.9}$$

where matrices $\mathbf{M}$, $\mathbf{C}$, and $\mathbf{G}$ are given below. The input $\mathbf{u_r} = [\mathbf{0}\ \mathbf{0}\ \mathbf{0}\ \mathbf{u_r}]^{\mathbf{T}}$ represents the motor force and $\mathbf{u} = [\mathbf{m_w}\ \mathbf{r_{px}}]^{\mathbf{T}}$ represents the ballast mass and battery position.

$$\mathbf{M}(\mathbf{q}, \mathbf{u}) = \begin{bmatrix} m_T & 0 & -\sum_{i=p,s,w} m_i \bar{z}_i & m_p c_\theta \\ 0 & m_T & \sum_{i=p,s,w} m_i \bar{x}_i & m_p s_\theta \\ -\sum_{i=p,s,w} m_i \bar{z}_i & \sum_{i=p,s,w} m_i \bar{x}_i & \sum_{i=p,s,w} m_i \left(\bar{x}_i^2 + \bar{z}_i^2\right) + J & m_p c_\theta \\ m_p c_\theta & m_p s_\theta & m_p c_\theta & m_p \end{bmatrix},$$

$$\mathbf{C}(\mathbf{q}, \dot{\mathbf{q}}, \mathbf{u}, \dot{\mathbf{u}}) = \begin{bmatrix} -2m_p s_\theta \dot{r}_{px}\dot{\theta} - \sum_{i=p,s,w} m_i \bar{x}_i \dot{\theta}^2 \\ -2m_p c_\theta \dot{r}_{px}\dot{\theta} - \sum_{i=p,s,w} m_i \bar{z}_i \dot{\theta}^2 \\ 2m_p r_{px}\dot{r}_{px} + K_{R2}\dot{\theta} \\ 2m_p \dot{\theta}\left(-s_\theta \dot{x}_p + c_\theta \dot{z}_p\right) \end{bmatrix},$$

$$\mathbf{G}(\mathbf{q}, \mathbf{u}) = \begin{bmatrix} F_d c_\xi + F_l sign(\alpha) s_\xi \\ F_d s_\xi - F_l sign(\alpha) c_\xi + m_T g - F_b \\ \sum_{i=p,s,w} m_i \bar{x}_i g \\ m_p g s_\theta \end{bmatrix}.$$

Note that the above dynamic models in (5.9) are similar to those in [13] with modification in hydrodynamic forces calculations in (5.9). Moreover, we use the Lagrangian approach, rather than the Newtonian method, to obtain the models, which are simpler for multi-body systems such as gliders [20].

5.3 EKF-Based Localization Design

In this section, we first present a reduced dynamic model and then an EKF-based localization design using the reduced dynamic model. Finally, we briefly discuss how to obtain the localization from the EKF design.

5.3.1 Reduced dynamic models

The control input u_r is difficult to obtain in the current glider system. So, we obtain the battery mass position and its derivatives instead. Therefore, variables r_{px}, $\dot{r}_{px}$ and $\ddot{r}_{px}$ are known and the last equation of (5.9) is not used for state estimations. We define system variables $\zeta = [\mathbf{x}\ \mathbf{z}\ \theta]^{\mathbf{T}}$ and then the first three equations of (5.9) can be re-written as

$$\mathbf{M_A}(\zeta, \mathbf{u})\ddot{\zeta} + \mathbf{C_A}(\zeta, \dot{\zeta}, \mathbf{u}, \dot{\mathbf{u}}) + \mathbf{G_A}(\zeta, \mathbf{u}) + \mathbf{R_{r_{px}}} = \mathbf{0}, \tag{5.10}$$

where matrices [1] $(\mathbf{M_A})_{ij} = (\mathbf{M})_{ij}$, $(\mathbf{C_A})_i = (\mathbf{C})_i$, $(\mathbf{G_A})_i = (\mathbf{G})_i$ for $i, j = 1, 2, 3$, and $\mathbf{R_{r_{px}}} = [\mathbf{m_p c}_\theta\ \ddot{\mathbf{r}}_{\mathbf{px}}\ \mathbf{m_p s}_\theta \ddot{\mathbf{r}}_{\mathbf{px}}\ \mathbf{m_p r_{pz}} \ddot{\mathbf{r}}_{\mathbf{px}}]^{\mathbf{T}}$.

We rewrite (5.10) into the state-space form as

$$\ddot{\zeta} = -\mathbf{M_A^{-1}} \left[\mathbf{C_A}(\zeta, \dot{\zeta}, \mathbf{u}, \dot{\mathbf{u}}) + \mathbf{G_A}(\zeta, \mathbf{u}) + \mathbf{R_{r_{px}}}\right]. \tag{5.11}$$

It is straightforward to obtain that

$$\begin{aligned} \det(\mathbf{M_A}) &= m_T^2 J + m_T \Big\{ m_h \sum_{i=p,s,w} m_i \left(\bar{x}_i^2 + \bar{z}_i^2\right) + \\ &\quad \sum_{i \neq j} m_i m_j \left[(\bar{x}_i - \bar{x}_j)^2 + (\bar{z}_i - \bar{z}_j)^2\right] \Big\} > 0 \end{aligned}$$

and therefore, $\mathbf{M_A}$ is always invertible. The glider dynamics (5.11) is complex to be used for attitude estimation and localization. Considering the fact that the battery movement is slow and only happens in short period, we approximate $\dot{r}_{px} \approx 0$ and $\ddot{r}_{px} \approx 0$. We define the state variable $\mathbf{x(t)} = [\mathbf{x}\ \dot{\mathbf{x}}\ \mathbf{z}\ \dot{\mathbf{z}}\ \theta\ \dot{\theta}]^{\mathbf{T}}$ and (5.11) can be reduced to

[1] We here omit the arguments in these coefficient matrices.

$$\dot{\mathbf{x}} = \mathbf{M_A^{-1}} \sum_{\mathbf{i=p,s,w}} \mathbf{m_i \bar{x}_i \dot{\theta}^2} - \mathbf{F_d c}_\xi - \mathbf{F_l s}_\xi$$
$$\sum_{i=p,s,w} m_i \bar{z}_i \dot{\theta}^2 - F_d s_\xi + F_l c_\xi - m_T g + F_b$$
$$-K_{R2}\dot{\theta} - \sum\nolimits_{i=p,s,w} m_i \bar{x}_i g$$

5.3.2 EKF design

We designed an EKF to estimate the state variables, especially the horizontal position x of the glider. For presentation clarity, we discuss the EKF design in discrete-time form. We define the state variable in discrete-time form as,

$$\mathbf{x(k)} = \begin{bmatrix} x(k) & \dot{x}(k) & z(k) & \dot{z}(k) & \theta(k) & \dot{\theta}(k) \end{bmatrix}^T$$

for $k \in \mathbb{N}$ and therefore, Eq. (5.12) is written as

$$\mathbf{x(k)} = \mathbf{x(k-1)} + \mathbf{T_s} \underbrace{\begin{bmatrix} x_2(k) \\ f_1(\mathbf{x(k)}, \mathbf{u(k)}) \\ x_3(k) \\ f_2(\mathbf{x(k)}, \mathbf{u(k)}) \\ x_5(k) \\ f_3(\mathbf{x(k)}, \mathbf{u(k)}) \end{bmatrix}}_{\bar{\mathbf{f}}(\mathbf{x(k)},\mathbf{u(k)})} + \omega(\mathbf{k}), \tag{5.12}$$

where T_s is the sampling time, $\omega_\mathbf{k}$ is the model uncertainties, and the control input $\mathbf{u(k)} = [\mathbf{m_w(k)}\ \mathbf{r_{px}(k)}]^\mathbf{T}$. The k-th observations include the depth and pitch angle measurements

$$\mathbf{y(k)} = \begin{bmatrix} z(k) \\ \theta(k) \end{bmatrix} + \mathbf{w_s(k)} = \mathbf{Hx(k)} + \mathbf{w_s(k)} \tag{5.13}$$

where $\mathbf{w_s(k)} \sim \mathcal{N}(\mathbf{0}, \sigma_\mathbf{s})$ is the sensor noise, $\sigma_\mathbf{s}$ is the covariance matrix for sensor measurements, and the matrix

$$\mathbf{H} = \begin{bmatrix} 0 & 0 & 1 & 0 & 0 & 0 \\ 0 & 0 & 0 & 0 & 1 & 0 \end{bmatrix}.$$

To design the EKF, we need to calculate the Jacobian matrix for the state equation. Since we treat input $\mathbf{u(k)}$ is known, the state equations do not have a separate term for $\mathbf{u(k)}$. Thus, the Jacobian matrix $\mathbf{F(k)}$ for (5.12) is obtained as

$$\mathbf{F(k)} = \begin{bmatrix} 1 \;\; T_s \;\; \mathbf{0_4} \\ \partial f_1(\mathbf{x},\mathbf{u})/\partial \mathbf{x} \\ \mathbf{0_2} \;\; \mathbf{1} \;\; \mathbf{T_s} \;\; \mathbf{0_2} \\ \partial f_2(\mathbf{x},\mathbf{u})/\partial \mathbf{x} \\ \mathbf{0_4} \;\; \mathbf{1} \;\; \mathbf{T_s} \\ \partial f_2(\mathbf{x},\mathbf{u})/\partial \mathbf{x} \end{bmatrix}_{\mathbf{x(k)},\mathbf{u(k)}} . \tag{5.14}$$

To calculate the above Jacobian matrix, we have to take the partial derivatives of function $\mathbf{f}(\mathbf{x},\mathbf{u})$ given in (5.12). Computing $\mathbf{f}(\mathbf{x},\mathbf{u})$ requires the calculation of $\det(\mathbf{M_A})$ given in (5.12). Note that the relative position variables $\bar{x}_i$ and $\bar{z}_i$, $i = p, s, w$, in (5.12) are not dependent on state variables x and z (i.e., the CB position). We can also treat θ as known in computing $\det(\mathbf{M_A})$ and therefore, we do not consider its state-dependency. Also angle ξ is a function of state variables given in (5.5) and can be written as $\xi = \arctan 2(x_4, x_2)$. In EKF implementation, we set $T_s = 0.1$ s, which is much less than measurements updating period (around 9-10 s). We design the following process in our EKF implementation. At the time we know both observations of the depth and the pitch angle, we can obtain the state estimation:

$$\hat{\mathbf{x}}(k|k-1) = \hat{\mathbf{x}}(k-1|k-1) + T_s \bar{\mathbf{f}}(\hat{\mathbf{x}}(k|k-1), \mathbf{u(k-1)}), \tag{5.15a}$$

$$\hat{\mathbf{x}}(k|k) = \hat{\mathbf{x}}(k|k-1) + \mathbf{W(k)}\left[\mathbf{y(k)} - \mathbf{H}\hat{\mathbf{x}}(\mathbf{k}|\mathbf{k-1})\right] \tag{5.15b}$$

and matrix $\mathbf{W(k)}$ is given as

$$\mathbf{W(k)} = \mathbf{P(k|k-1)H^T}\left[\mathbf{HP(k|k-1)H^T} + \mathbf{R(k)}\right]^{-1}.$$
$$\mathbf{P(k|k-1)} = \mathbf{F(k)P(k-1|k-1)F(k)^T} + \mathbf{Q(k-1)},$$
$$\mathbf{P(k|k)} = [\mathbf{I_6} - \mathbf{W(k)H}]\,\mathbf{P(k|k-1)}.$$

If no measurement is obtained then the states estimation just involves with the current control input with the last step estimates. If we obtain only one sensor measurement, either the depth or the pitch angle, we still use (5.15) to update the state estimates with output matrix $\mathbf{H_1}$ or $\mathbf{H_2}$, the first or the second row vectors of $\mathbf{H}$, respectively [20].

5.3.3 Localization computing

With the estimated EKF-based horizontal velocity $\hat{\dot{x}}$, we compute the glider's position by using the heading angle $\phi(t)$ obtained from the attitude sensor. We assume that the glider's velocity is in the vertical plane (i.e., zero side slip angle $\beta = 0$.) For comparison purposes, we also compute the dead reckoning-based localization. The dead reckoning results are calculated similar to that of the above discussion. But in dead reckoning method $\hat{\dot{x}}$ is estimated by using the vertical velocity $\hat{\dot{z}}$ from the altimeter and the pitch angles are estimated with an assumption that the glider's velocity is along its heading direction, that is, $\hat{\dot{x}} = \hat{\dot{z}}\cot\theta$. We will show the results in the next section [20].

5.4 Experimental Results

In this section, we first describe the glider deployments and the experimental data that we use in this study. Then we present the experimental model validation and show the localization results.

5.4.1 Glider deployments

We use two data sets that were obtained in a glider deployment which started on July 22, 2010 by the RUCOOL. Fig. deploy shows the glider trajectory for the mission. The mission started from the south New Jersey coast near Rutgers Tuckerton Field Station. The total distance the glider (RU21) traveled was around 183 km. We choose two portions of the

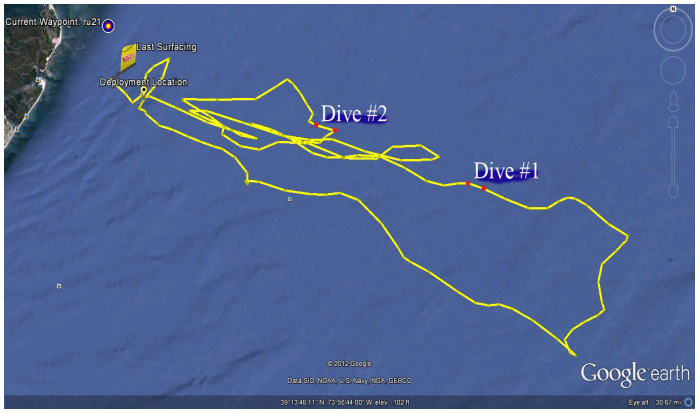

Figure 5.3: The Google Earth map of the glider deployments in July 2010. The two data sets (Dives #1 and #2) we use in this study are marked by two pairs of red dots on the glider trajectory [20]

trajectory, as shown between two pairs of red dots marked on the trajectory in Fig. deploy. Both portions are between two adjacent glider surface points so that we have GPS waypoints at the beginning and the ending points of each dive. In Dive #1, the glider ran 1.39 km for about 121 minutes before it surfaced again, while in Dive #2, the glider ran 1.61 km for about 119 minutes. The chosen trajectories are relatively straight and it may fit our assumption that glider's lateral dynamics do not play a significant role here if we do have a 3D model or experimental data to back this assumption [20].

Table 5.1: The physical parameters for RU21 glider [20].

m_h(kg)	m_p(kg)	m_w(kg)	m_s(kg)	J(kgm^2)	r_{px}(m)	r_{pz}(m)
50	9.1	0.46	1.0	19.6	0.495	-0.029
r_{sx}(m)	r_{sz}(m)	ρ(kg/m^3)	A(m^2)	V(liter)	r_{wx}(m)	r_{wz}(m)
0	-0.029	1030	0.0355	59.991	0.9	0

The RU21 was a shallow water glider equipped with standard navigation sensors such as altimeter, attitude sensors, and GPS etc. During the mission, the glider was also equipped with a DVL sensor to measure the velocity of the glider and the ocean current. The DVL also measures the glider positions. The model parameters for RU21 are either measured or estimated, as listed in Table 5.1 and Table 5.2.

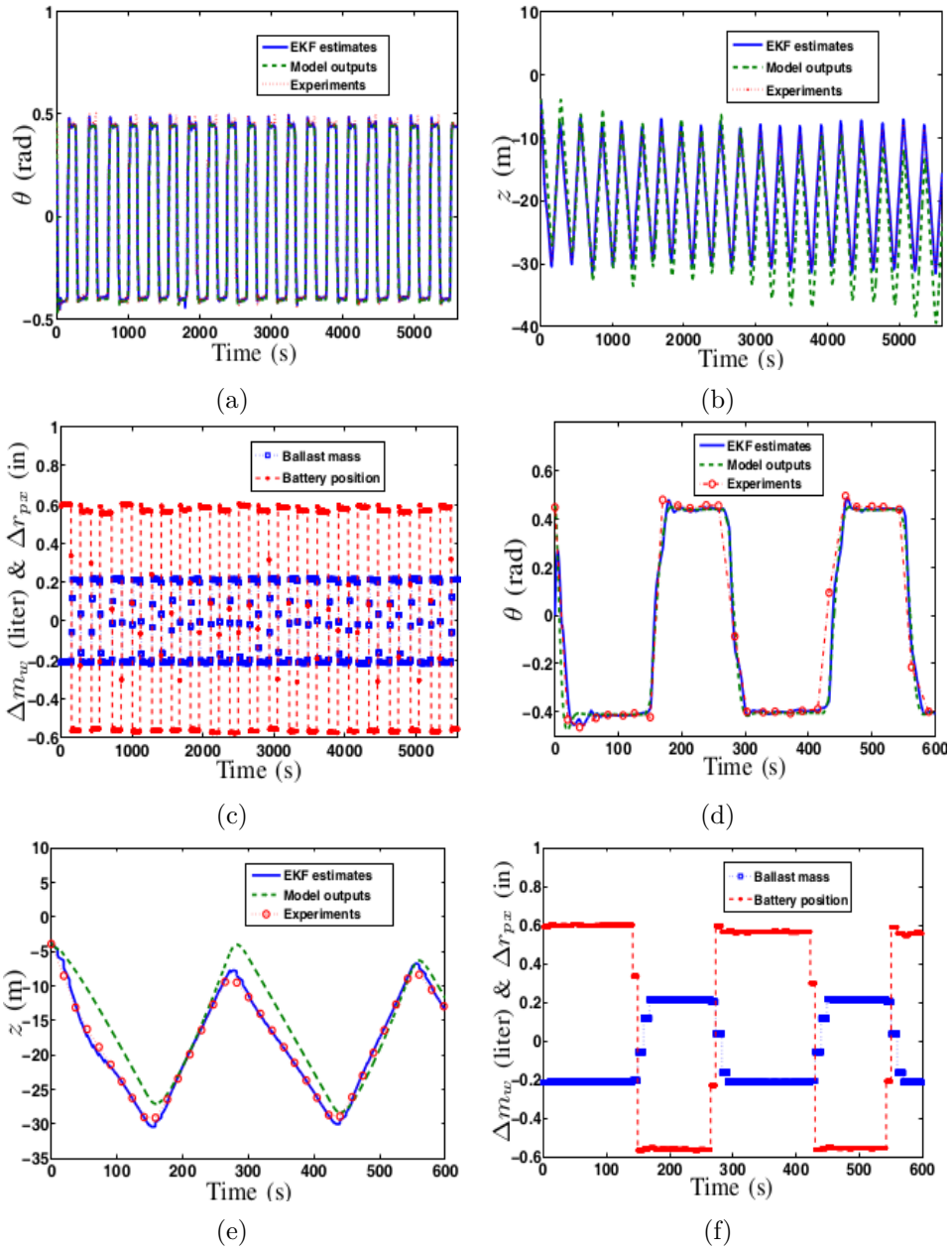

Figure 5.4: The glider's motion comparison of the dynamic model-based estimation, the EKF-based estimation and the experimental measurements between two surfacing waypoints in the deployment 1. (a) The pitch angle θ for the entire period. (b) The glider depth z for the entire period. The negative value for z means underneath the sea surface. (c) The glider inputs: the ballast mass changes Δm_w (in liter) and the battery position changes $\Delta r_p x$. (d) The zoomed pitch angle θ over the first 10 mins. (e) The zoomed glider depth z over the first 10 mins. (f) The zoomed control inputs over the first 10 minutes [20].

Table 5.2: The modeling parameters for RU21 glider in deployments [20]

K_L^+	K_L^-	K_{D0}	K_{D1}^+	K_{D1}^-	K_{R1}^+	K_{R1}^-	K_{R2}
5.13	6.63	0.05	6.3	6.25	1.35	0.45	-20

5.4.2 Model validation

We take the measurement data in Dive #1 for model validation. Fig. 5.4 shows the comparison results of the model prediction of the glider's pitch angle θ Fig. 5.4(a) and (d), and the diving depth z Fig. 5.4 (b) and (e) profiles with their respective experimental data. The control inputs, the ballast mass m_w and the battery position r_{px}, are also plotted Fig. 5.4(c) and (f).

We calculate the model outputs by using (5.10) and the control inputs shown in Fig. 5.4(c). The model output plots shown in Fig. 5.4 clearly match the system outputs in Dive #1. These comparison results confirm that the proposed dynamic models capture the basic motion of the Slocum glider [20].

5.4.3 Localization experiments

Fig. 5.5 shows the comparison results of the localization in Dives #1 and #2 by dead reckoning, dynamic model prediction, EKF-based localization, and DVL measurements. We consider the DVL-based localization as the ground truth and compare it with the localization results by the other methods. The localization results marked as the model outputs shown in Fig. 5.5 are obtained by using the outputs of the glider dynamic model (5.10) with the known control inputs in experiments [20].

From Fig. 5.5, we found that the proposed EKF-based localization scheme predicts much better positioning information than those given by the dead reckoning for both Dives #1 and #2. Comparing with the ground truth positioning given by DVL, the EKF-based localization results have some errors and we will discuss the reasons for such a difference. It is also interesting to observe that the positioning information by directly using glider's dynamic model also provides a much better results than those by dead reckoning though in general they are worse than the results by the EKF-based localization approach [20].

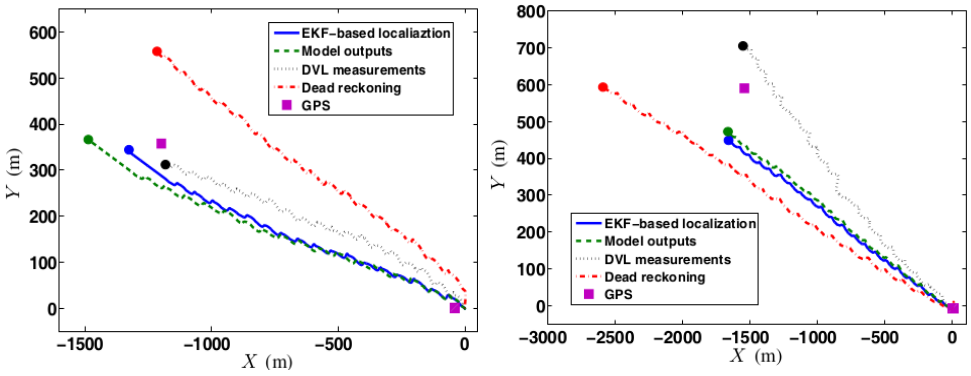

(a) (b)

Figure 5.5: Localization comparisons under various methods. (a) Dive #1 (b) Dive #2 [20].

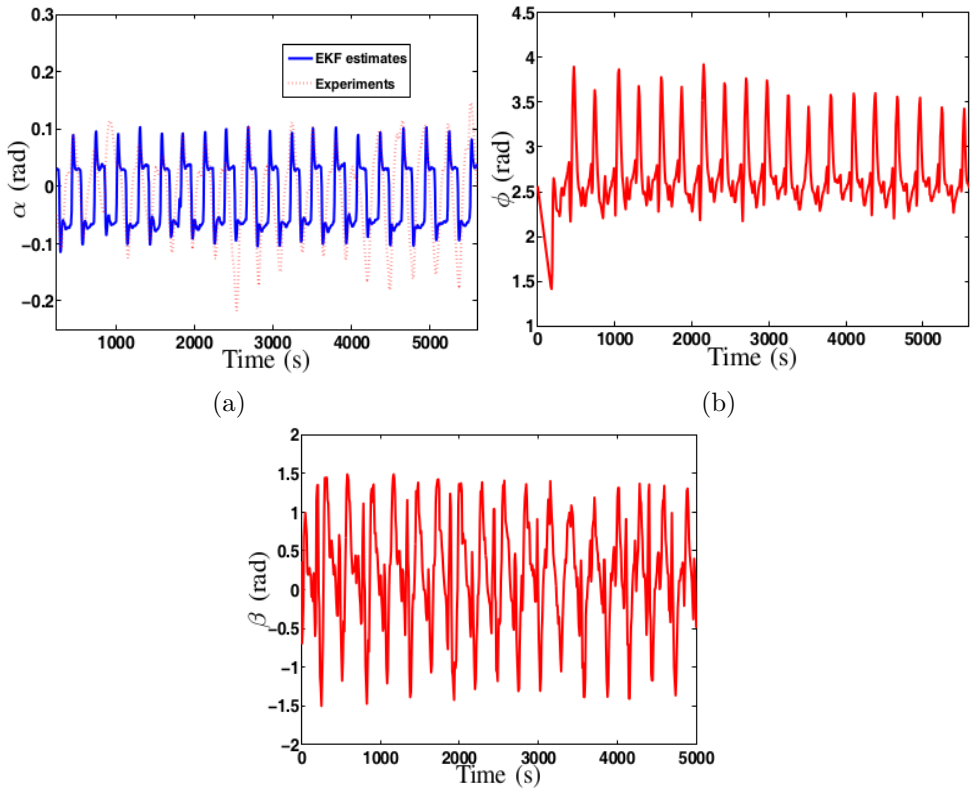

(a) (b)

(c)

Figure 5.6: (a) The EKF-based estimates and DVL-based calculations of attack angle α for Dive #1. (b) Heading angle ϕ and (c) calculated side slip angle β for Dive #1 [20].

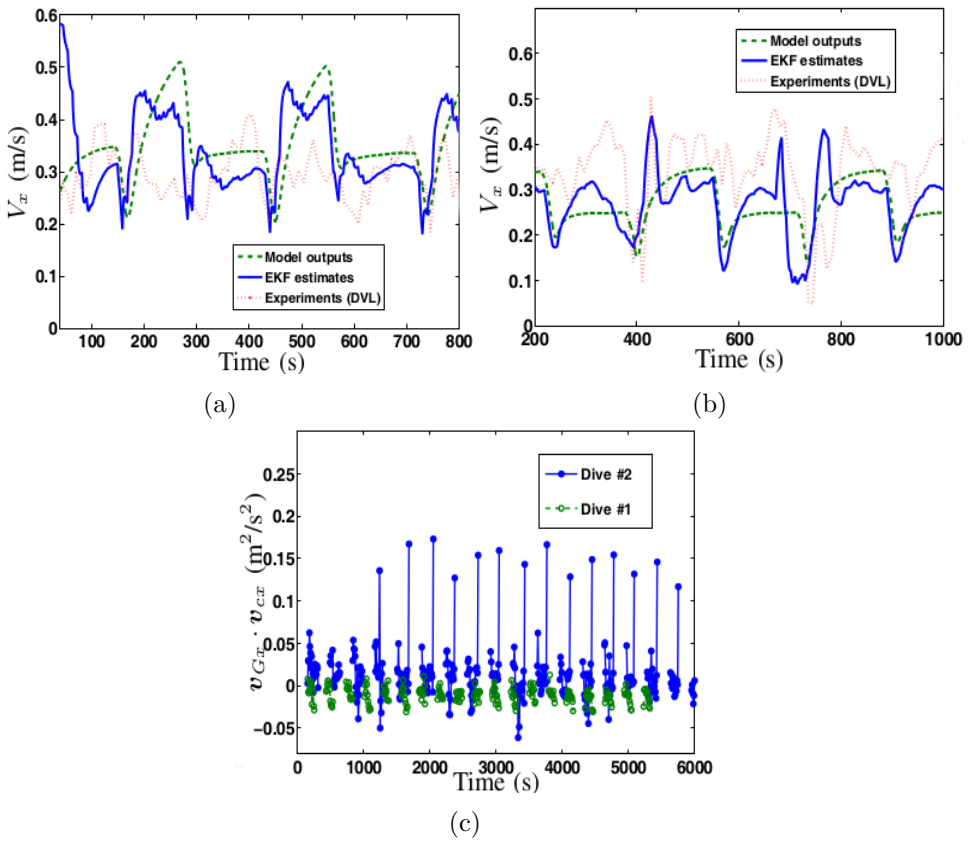

Figure 5.7: The glider's horizontal velocity comparisons (longitudinal direction) of the dynamic model-based estimation, the EKF-based estimation and the experimental measurements by DVL. (a) Dive #1. (b) Dive #2. (c)Comparison of $\mathbf{v_{Gx}} \cdot \mathbf{v_{cx}}$ for Dives #1 and # 2 [20].

Both the dynamic model outputs and the EKF-based localization approach perform better than the dead reckoning. One of the main reasons for such superior performance is that they are based on the glider dynamics, which consider the fact that the glider's velocity direction is not aligned with the heading direction, i.e., there exists a nonzero attack angle α. Fig. 5.6 shows the calculations of α by the EKF approach (blue solid line) and also by the DVL and depth measurements (red dashed line). The attack angle α is nonzero (between -0.1 and 0.1 rads) in Dive #1 [20].

5.4.4 Discussions

The comparison results show that there are some differences between the EKF-based localization and the actual glider positioning. The main reasons for these differences are due to the influences of ocean currents and the lateral motions of the glider.

Fig. 5.7(a) and (b) show the EKF-based and dynamic model estimates and DVL measurements of the glider's horizontal velocity magnitude V_x for Dives #1 and #2, respectively. For Dive #1, V_x estimates by the EKF (blue solid lines) and the dynamic model (green dashed lines) are in general larger than actual glider horizontal speed (red dotted lines), while for Dive #2, the actual glider's velocity is larger than those estimates. The differences between the estimates and the actual velocities come from the fact that in Dive #1, the ocean current velocity is roughly in the reverse direction of glider movement, while in Dive #2, the ocean current moves roughly along the same direction as the glider's longitudinal motion. We do not include the ocean currents in the dynamic models and therefore, the estimates of both the dynamic model and the EKF approaches do not capture the influence of the ocean currents. We further confirm this by plotting the dot product of the ocean currents horizontal velocity vector $\mathbf{v_{cx}}$ and the glider's horizontal velocity vector $\mathbf{v_{wx}}$ for both dives, as shown in Fig. 5.6. We clearly see that for Dive #2, $\mathbf{v_{Gx}} \cdot \mathbf{v_{cx}} > \mathbf{0}$ for most time and for Dive #1, $\mathbf{v_{Gx}} \cdot \mathbf{v_{cx}} < \mathbf{0}$. These calculations confirm that the ocean currents help the glider move faster in Dive #2 and slow down the glider in Dive #1 [20].

Another source that brings the EKF-based localization errors is the neglection of glider's lateral dynamics in the design. We assume that glider's motion is restricted in the vertical plane, i.e., zero side slip angle $\beta = 0$. However, this is not the case for both Dives #1 and #2. For example, Fig. 5.6 (b) and (c) show the glider's heading angle ϕ and side slip angle β for Dive #1. Clearly, the glider moves laterally with a large nonzero β (between -1.5 and 1.5 rads) in Dive #1. For more accurate localization, we need to capture the lateral dynamics in the EKF design [20].

Chapter 6

Conclusion and Future Work

6.1 Conclusion

We have demonstarted the working of our prototype and the results that we have obtained going right upto the final stage of doing analysis of the biomass. The analysis gave us a proof of our system being able to perform filtration and purging as required. We have also conducted contamination and preservation tests to validate our system for cross contamination and preservation. The results confirmed that the bio-sampler was able to perform preservation of the sample. Also the sample profiles confirmed that the bio-sampler did not cause any cross-contamination between the samples. These are very basic and important criteria to be satisfied by the bio-sampler. Cross contamination would lead to the entire sampling process for two or more filters being of no use for doing analysis. The idea of collecting samples while the underwater glider goes through different location is completely defeated when we observe cross contamination. Hence from our design by being within the limits of contamination and being able to preserve the sample, we have given a proof of concept that can be considered as a basis for the next glider version.

As the second part of the thesis, we also presented a dynamic model-aided localization scheme for Slocum underwater autonomous gliders. The proposed localization method was built on the glider dynamic model with the known control inputs and the on-board sensor measurements such as the depth and the pitch angle. Therefore, one attractive advantage of the new localization approach is that no any additional sensors is needed to be installed on gliders. Using the new dynamic model, we presented an EKF-based glider positioning and motion estimation. We compared the results with the experimental data obtained in glider deployments. The results confirmed that the new localization scheme performed much better than those by the commonly used dead reckoning. The results also confirmed

that the unmodeled ocean currents and the glider's lateral dynamics are the most influential factors contributed to the localization errors.

6.2 Future Work

The future work is directed towards designing the bio-sampler which would be mounted in the science bay of the glider.

The challenges that we foresee are listed below:

- The size of the bio-sampler to be accommodated within the limited space in the glider
- Reduce the number of movable parts
- How the bio-sampler system would behave in a vacuum environment considering the fact that the entire glider interior is cleared out of air and has a vacuum environment before any mission.
- Problem of having limited air to dry the filters inside the gilder
- The way we handle the inlet of water from outside the glider and into the bio-sampler since there would be a huge pressure differential at different depths underwater.

The basis for these challenges is that we are using water pumps, air & water tight clamp, water lines, air lines and also the air pump. These are working at different pressure differences at different stages while filtering, purging and drying. Hence it is worthwhile to think that there would be design challenges that we may face while this whole system is inside a vacuum environment and sealed from the outside world and under pressure while operating at great depths underwater.

Also further improving the glider localization can be achieved by extending the current model to a 3D model for the glider. This would include the effects of ocean currents and lateral motion. The proposed positioning scheme is planned to be used to estimate ocean currents simultaneously with additional inertial sensors such as inertia measurement units (IMU).

Interestingly as a spin-off of the main design that would go on-board the glider, this table-top version of the bio-sampler also has huge potential to be used in any lab or field environment. Maintaining the same principle of operation but slight modifications in design would make this bio-sampler versatile enough to be used in different applications such as a medical device for analyzing blood samples. Another potential application could be in qualitative analysis of ground water which would further let us understand the impacts during early stages of site planning and provide a cost-effective method to asses environmental impacts. There are numerous studies that reveal the factors influencing the health of people with the ground water used by them [21]. The bio-sampler would ease the procedure of analysis for scientists by providing them an autonomous platform to sample water and preserve it in time from any degradation. Similarly improvements in robustness and repeatability of the performance of this prototype would also help in development of a field version which can be deployed next to a river, a lake or any other water body of interest to the marine scientists.

Appendix A

Python Code

```
Code used upto the stage of 2nd set of contamination tests.
Last Update Date : March 17, 2014
Code updates:
1. Code set-up for doing 2nd contamination and preservation tests.
2. Manipulating the clamp to a user defined filter location
3. Getting user input to choose an
action after manipulating to a filter location
######### INCULDING Gumstix (CONTROLLER) LIBRARIRES #########
from robovero.extras import Array, roboveroConfig
from robovero.internals import resetConfig
from robovero.LPC17xx import *
from robovero.lpc17xx_uart *
from robovero.lpc_types import TRANSFER_BLOCK_Type, FunctionalState
from robovero.arduino import *
from robovero.lpc17xx_pwm import *
from robovero.lpc17xx_qei import*
from robovero.lpc17xx_pinsel import *
from robovero.lpc17xx_clkpwr import *
from time import sleep
import serial
import time
import sys
from datetime import datetime
```

```
################### DEFINE DI/DO'S ###############
pinMode(P0_4, INPUT)
pinMode(P0_5, INPUT)
pinMode(P0_20, INPUT)
pinMode(P1_27, INPUT)
pinMode(P4_28, INPUT)
pinMode(P4_29, INPUT)
pinMode(P2_3, OUTPUT)
pinMode(P2_4, OUTPUT)
pinMode(P2_6, OUTPUT)
pinMode(P2_8, OUTPUT)
pinMode(P2_10, OUTPUT)
pinMode(P0_19, OUTPUT)
################## PWM ##########################
def initPulse(channel, pulse_width):
  initMatch(channel, pulse_width)
def initPeriod(period):
  initMatch(0, period)
################## PWM1 #########################
def initPWM1():
  # Set the period to 800us = 0.8ms = 1250Hz
  initPeriod(200)
  # Set the pulse width to 0.4ms
  initPulse(1,800)
  PWM_ChannelCmd(LPC_PWM1, 1, FunctionalState.ENABLE)
  PWM_ResetCounter(LPC_PWM1)
  PWM_CounterCmd(LPC_PWM1, FunctionalState.ENABLE)
  PWM_Cmd(LPC_PWM1, FunctionalState.ENABLE)
def pwm1_do_ON():
```

```
  while True:
    match_value = 200   # For changing duty cycle
    if match_value:
      PWM_MatchUpdate(LPC_PWM1, 1, match_value,
       PWM_MATCH_UPDATE_OPT.PWM_MATCH_UPDATE_NOW)
      time.sleep(0)
    break
  return match_value
def pwm1_do_OFF():
  while True:
    match_value = 10   # For changing duty cycle
    if match_value:
      PWM_MatchUpdate(LPC_PWM1, 1, match_value,
        PWM_MATCH_UPDATE_OPT.PWM_MATCH_UPDATE_NOW)
      time.sleep(0)
    break
  return match_value
##################################################
################# PWM2 ############################
def initPWM2():
  # Set the period to 800us = 0.8ms = 1250Hz
  initPeriod(200)
  # Set the pulse width to 0.4ms
  initPulse(1,800)
  PWM_ChannelCmd(LPC_PWM1, 2, FunctionalState.ENABLE)
  PWM_ResetCounter(LPC_PWM1)
  PWM_CounterCmd(LPC_PWM1, FunctionalState.ENABLE)
  PWM_Cmd(LPC_PWM1, FunctionalState.ENABLE)
def pwm2_do_ON():
  while True:
```

```
    match_value = 200   # For changing duty cycle
    if match_value:
      PWM_MatchUpdate(LPC_PWM1, 2, match_value,
        PWM_MATCH_UPDATE_OPT.PWM_MATCH_UPDATE_NOW)
      time.sleep(0)
    break
  return match_value
def pwm2_do_OFF():
  while True:
    match_value = 10   # For changing duty cycle
    if match_value:
      PWM_MatchUpdate(LPC_PWM1, 2, match_value,
        PWM_MATCH_UPDATE_OPT.PWM_MATCH_UPDATE_NOW)
      time.sleep(0)
    break
  return match_value
################################################################################
roboveroConfig()
initPWM1()
initPWM2()
################### UART 1 CONFIG START ######################################
UARTConfigStruct = UART_CFG_Type()
UART_ConfigStructInit(UARTConfigStruct.ptr);
UARTConfigStruct.Baud_rate = 38400;
UART_Init(LPC_UART1, UARTConfigStruct.ptr);
UART_TxCmd(LPC_UART1,1);
################### UART 1 CONFIG END ########################################
################### UART 2 CONFIG START ######################################
UARTConfigStruct = UART_CFG_Type()
UART_ConfigStructInit(UARTConfigStruct.ptr);
```

```
UARTConfigStruct.Baud_rate = 38400;
UART_Init(LPC_UART2, UARTConfigStruct.ptr);
UART_TxCmd(LPC_UART2,1);
################### UART 2 CONFIG END ########################################
def abort_sequence():
  stop_command()
  digitalWrite(P2_3, LOW)  # Valve D
  digitalWrite(P2_4, LOW)  # Valve A
  digitalWrite(P2_6, LOW)  # Valve C
  digitalWrite(P2_8, LOW)  # Water Pump
  digitalWrite(P2_10, LOW) # SV4
  digitalWrite(P0_19, LOW) # Air Pump
  print "All DOs OFF"
  sys.exit("EXIT... End of program due to an error!!!")
############ MAIN MOTOR FORWARD / REVERSE COMMANDS ############################
def stop_command():
  _msg = 0b0
  #print "STOP"
  msg = Array(len(str(_msg)), 1, _msg)
  UART_Send(LPC_UART1, msg.ptr, msg.length, TRANSFER_BLOCK_Type.BLOCKING)
def forward_command():
  _msg = 0b1011010
  #print "FORWARD",_msg
  msg = Array(len(str(_msg)), 1, _msg)
  UART_Send(LPC_UART1, msg.ptr, msg.length, TRANSFER_BLOCK_Type.BLOCKING)
def reverse_command():
  _msg = 0b10100
  #print "REVERSE",_msg
  msg = Array(len(str(_msg)), 1, _msg)
  UART_Send(LPC_UART1, msg.ptr, msg.length, TRANSFER_BLOCK_Type.BLOCKING)
```

```
############ LINEAR ACTUATOR FORWARD / REVERSE COMMANDS ######################
def la_stop_command():
  _msg = 0b1111111
  #print "STOP"
  msg = Array(len(str(_msg)), 1, _msg)
  UART_Send(LPC_UART2, msg.ptr, msg.length, TRANSFER_BLOCK_Type.BLOCKING)
def up_command():
  _msg = 0b11110000
  #print "UP",_msg
  msg = Array(len(str(_msg)), 1, _msg)
  UART_Send(LPC_UART2, msg.ptr, msg.length, TRANSFER_BLOCK_Type.BLOCKING)
def down_command():
  _msg = 0b11
  #print "DOWN",_msg
  msg = Array(len(str(_msg)), 1, _msg)
  UART_Send(LPC_UART2, msg.ptr, msg.length, TRANSFER_BLOCK_Type.BLOCKING)
############ CLAMP MOTOR OPEN / CLOSE COMMANDS ##############################
def open_clamp():
  _msg = 0b11110000
  print "clamp opening"
  #print "OPEN",_msg
  msg = Array(len(str(_msg)), 1, _msg)
  UART_Send(LPC_UART1, msg.ptr, msg.length, TRANSFER_BLOCK_Type.BLOCKING)
def close_clamp():
  _msg = 0b10001100
  #print "CLOSE",_msg
  msg = Array(len(str(_msg)), 1, _msg)
  UART_Send(LPC_UART1, msg.ptr, msg.length, TRANSFER_BLOCK_Type.BLOCKING)
  while True:
    b = digitalRead(P1_27)
```

```
    #print " b = ", b
    if b == 0:
      time.sleep(0) # tightening the inside clamp more by incr time
      stop_command()
      print "Clamp Closed"
     break
######################### HOMING COMMANDS ################################
def linear_actuator_homing():
  down_command()
  print "Linear Actuator homing..."
  while True:
    b = digitalRead(P4_28)
    #print " b = ", b
    if b == 0:
      time.sleep(0) # lower the linear actuator more by incr time
                    # (be careful since this is accumulative
                    #  if its already in home position)
      la_stop_command()
      print "Linear Actuator at home"
      break
def central_disc_homing():
  forward_command()
  print "Homing..."
  while True:
    a = digitalRead(P0_5)
    #print "a = ", a
    if a == 0:
      stop_command()
      print "Central disc at home position"
      break
```

```
def clamp_homing():
  open_clamp()
  while True:
    b = digitalRead(P0_20)
    #print " b = ", b
    if b == 0:
      time.sleep(0)
      stop_command()
      print "Clamp at home position"
      break
def filter_pos():
  forward_command()
  time.sleep(0.3) # to come out of the limit switch
                  # current state else it will stop there itself
  while True:
    b = digitalRead(P0_4)
    #print " b = ", b
    if b == 0:
      stop_command()
      time.sleep(1)
      break
###################### SPITTING ########################
def short_spit():
  time.sleep(1)
  digitalWrite(P2_3,LOW)
  time.sleep(0.5)
  digitalWrite(P2_3,HIGH)
  print "short spit"
  time.sleep(1)
def long_spit():
```

```
  time.sleep(1)
  digitalWrite(P2_3,LOW)
  time.sleep(2)
  digitalWrite(P2_3,HIGH)
  print "long spit"
  time.sleep(1)
def spitting():
  print "Spitting started"
  digitalWrite(P2_6,LOW)      # open flow of the pump for effective spitting
  print "Open Valve C"
  for x in range (1,10):
    short_spit()              # a sequence of 10 short spits
  print "Spitting done"
############ FILTER AND PURGE ONLY ######################
def filter_purge():
# filtering
  print "Filter and purge starts..."
  pwm1_do_ON()
  print "Valve B open"
  pwm2_do_ON()
  print "Valve E open"
  digitalWrite(P2_8,HIGH)
  print "Water Pump ON"
  print "Filtering..."
  time.sleep(20)
# purge
  digitalWrite(P2_10,HIGH)
  print "SV4 ON"
  print "Purging..."
  time.sleep(70)
```

```
  digitalWrite(P2_10,LOW)
  print "SV4 OFF"
  digitalWrite(P2_8,LOW)
  print "Water Pump OFF"
  pwm1_do_OFF()
  print "Valve B close"
############## DRYING ###################################
def drying():
  print "Drying starts..."
  open_clamp()
  time.sleep(3.5)
  stop_command()
  print "Open valve D"
  digitalWrite(P2_3,HIGH)
  time.sleep(1)
  digitalWrite(P0_19,HIGH)
  print "Air Pump ON"
  time.sleep(1)
  spitting()
  print "let spitted water out"
  time.sleep(10)
  pwm2_do_OFF()
  print "Valve E close"
#drying
  print "Drying..."
  digitalWrite(P2_4,HIGH)
  print "Valve A ON"
  time.sleep(1)
  print "Close Valve B"
  time.sleep(1)
```

```
  spitting()
  print "Close Valve C"
  digitalWrite(P2_6,HIGH)
  time.sleep(300)
  spitting()
  print "Close Valve C"
  digitalWrite(P2_6,HIGH)
  time.sleep(300)
  digitalWrite(P2_3,LOW)
  print "Valve D OFF"
  digitalWrite(P2_4,LOW)
  print "Valve A OFF"
  digitalWrite(P2_6,LOW)
  print "Valve C OFF"
  digitalWrite(P0_19,LOW)
  print "Air Pump OFF"
  print "Drying Complete"
  time.sleep(1)
################## PRIMING ##############################
def priming_start():
  print "Priming started"
  digitalWrite(P2_8,HIGH)
  print "Water Pump ON"
  pwm1_do_ON()
  print "Valve B open"
  print "Filtering..."
  time.sleep(20)
# purge the water out
  digitalWrite(P2_10,HIGH)
  print "SV4 ON"
```

```
  print "Purging..."
  time.sleep(20)
  digitalWrite(P2_10,LOW)
  print "SV4 OFF"
  time.sleep(1)
  digitalWrite(P2_8,LOW)
  print "Water Pump OFF"
  time.sleep(1)
  print "Priming completed"
  pwm1_do_OFF()
  print "Valve B close"
  time.sleep(0)
def priming():
  print "Priming starts..."
  priming_start()
  time.sleep(1)
  clamp_homing()
def filter_purge_dry():
  print "Filter purge drying starts..."
  filter_purge()
  drying()
  print "filt purge dry"
### GET USER INPUT TO CHOOSE WHAT IS TO BE DONE NEXT ###
def what_to_do():
  print " \n Choose what to do next: \n Filter & Purge - 1
  \n Drying - 2 \n Both - 3 \n Priming - 4 \n"
  choice = int(raw_input("Enter your choice : "))
process = { 1 : filter_purge, 2: drying, 3: filter_purge_dry, 4: priming,}
process[choice]()
def clamp_open_close():
```

```
  clamp_homing()
  time.sleep(1)
  close_clamp()
  time.sleep(1)
  what_to_do()
  time.sleep(1)
  clamp_homing()
def filter_ring_location(i):
  print "Filter number", i ,"chosen \n"
  for x in range (1,i + 1):
    print x
    filter_pos()
  clamp_open_close()
  central_disc_homing()
############### RUNNING OF CODE STARTS HERE ######################
################# SET ALL OUTPUTS TO OFF STATUS ###################
stop_command()
pwm1_do_OFF()  # Valve B
pwm2_do_OFF()  # Valve E
digitalWrite(P2_3, LOW)  # Valve D
digitalWrite(P2_4, LOW)  # Valve A
digitalWrite(P2_6, LOW)  # Valve C
digitalWrite(P2_8, LOW)  # Water Pump
digitalWrite(P2_10, LOW) # SV4
digitalWrite(P0_19, LOW) # Air Pump
print "All DOs OFF"
############## GET USER INPUT FOR FILTERING LOCATION ###############
filter_bracket = int(raw_input("Enter filter bracket number(1 or 2):"))
filter_number = int(raw_input("Enter filter number (1 to 8):"))
############## HOME ALL THE THREE DEGREES OF FREEDOM ###############
```

```
clamp_homing()
central_disc_homing()
time.sleep(1)


if filter_bracket == 1:
  linear_actuator_homing()
else:
  print "."
########## MANIPULATING THE CLAMP TO THE SET FILTER LOCATION #################
def lin_act_bracket1():
  up_command()
  data_old = 0
  count = 0
  while True:
    a = digitalRead(P4_29)
    #print a
    if a == 0:
      time.sleep(0)
      #print "Filter bracker", x
      la_stop_command()
      time.sleep(1)
      break
def bracket_1():
  print "Filter bracket 1 chosen \n"
  filter_ring_location(filter_number)
def bracket_2():
  print "Filter bracket 2 chosen \n"
  lin_act_bracket1()
  filter_ring_location(filter_number)
def bracket_3():
```

```
  print "Filter bracket 3 chosen \n"
  lin_act_bracket1()
  filter_ring_location(filter_number)
def bracket_4():
  print "Filter bracket 4 chosen \n"
  lin_act_bracket1()
  filter_ring_location(filter_number)
bracket = { 1 : bracket_1, 2: bracket_2, 3: bracket_3, 4: bracket_4,}
bracket[filter_bracket]()
########## END THE PROGRAM WITH SETTING THE OUTPUTS TO OFF STATUS ###########
stop_command()
pwm1_do_OFF()  # Valve B
pwm2_do_OFF()  # Valve E
digitalWrite(P2_3, LOW)  # Valve D
digitalWrite(P2_4, LOW)  # Valve A
digitalWrite(P2_6, LOW)  # Valve C
digitalWrite(P2_8, LOW)  # Water Pump
digitalWrite(P2_10, LOW) # SV4
digitalWrite(P0_19, LOW) # Air Pump
print "All DOs OFF & EXIT!!!"
```

References

[1] http://www.dosits.org/technology/observermarineanimals/acousticgliders/

[2] O. Schofield, J. Kohut, D. Aragon, L. Creed, J. Graver, C. Haldeman, J. Kerfoot, H. Roarty, C. Jones, D. Webb, and S. Glenn Slocum gliders: Robust and ready *J. Field Robotics*, vol. 24, no. 6, pp. 473 - 485, 2007.

[3] E. Hudson Ocean gliders - Technology, eleconomics drivers, and roadmap *Proc. IEEE/MTS OCEANS Conf., Waikoloa, HI,*,2011.

[4] D. Rudnick, R. E. Davis, C. C. Eriksen, D. M. Fratantoni, and M. J. Perry Underwater gliders for ocean research *Marine Technol. Soc. J.*, vol. 38, no. 2, pp. 73 - 84, 2004.

[5] http://www.ag.auburn.edu/fish/image_gallery/details.php?image_id=1713

[6] http://www.halltechaquatic.com/kemmerer-water-samplers/95.html

[7] http://www.marinebio.net/marinescience/01intro/tosamp.htm

[8] Ryan JP, Johnson SB, Sherman A, Rajan K, Py F, Thomas H et al. Mobile autonomous process sampling within coastal ocean observing systems. *Limnol. Oceanog. Methods*, 8: 394 - 402, 2010.

[9] The MBARI Environmental Sample Processor (ESP). Illustrations describing the ESP available online at http://www.mbari.org/esp/

[10] http://rucool.marine.rutgers.edu/COOL-Research/biotic-infrastructure-for-ocean-microbial-ecology-biome-sampler

[11] http://www.mobio.com/dna_fragment_in_solution/ultraclean-15-dna-purification-kit.html

[12] Rutgers University Coastal Ocean Observation Lab (RUCOOL), http://rucool.marine.rutgers.edu

[13] J. G. Graver, Underwater gliders: Dynamics, control and design Ph.D. dissertation, Dept. Mech. Aero. Eng., Princeton Univ., Princeton, NJ, 2005.

[14] D.R.Thompson, S.Chien, Y.Chao, P.Li, B.Cahill, J.Levin, O.Schofield, A.Balasuriya, S.Petillo, M.Arrott, and M.Meisinger, Spatiotemporal path planning in strong, dynamic, uncertain currents *Proc. IEEE Int. Conf. Robot. Autom.,*, Anchorage, AK, 2010, pp. 4778-4783.

[15] R.N.Smith, J.Kelly, and G.S.Sukhatme, Towards improving mission execution for autonomous gliders with an ocean model and Kalman filter, *Proc. IEEE Int. Conf. Robot. Autom.,*, St. Paul, MN, 2012, pp. 4870-4877.

[16] N. Mahmoudian, J. Geisbert, and C. Woolsey, Approximate analytical tuning conditions for underwater gliders: Implication for motion control and path planning, *IEEE J. Oceanic Eng.,*, vol. 35, no. 1, pp. 131-143, 2010.

[17] H. C. Woithe, D. Boehm, and U. Kremer, Improving Slocum glider dead reckoning using a Doppler Velocity Log, *Proc. IEEE/MTS OCEANS Conf.*, Waikoloa, HI, 2011.

[18] O. Hegrenaes and O. Hallingstad, Model-aided INS with sear current estimation for robust underwater navigation *IEEE J. Oceanic Eng.,*, vol. 36, no. 2, pp. 316âĂŞ337, 2011.

[19] http://auvac.org/configurations/view/49

[20] P. Wang, P. K. Singh, J. Yi, Dynamic model-aided localization of underwater autonomous gliders *IEEE Conference on Robotics and Automation (ICRA)*, 5565 - 5570, 2013.

[21] T. Rango, J. Kravechenko, B. Atlaw, P.G. Cornick, M. Jeuland, B. Merola, A. Vengosh Groundwater quality and its health impact: An assessment of dental fluorosis in rural inhabitants of the Main Ethiopian Rift *Environment International*, vol. 43, pp. 37 - 47, 2012.